N95- 32237

TDA Progress Report 42-121

May 15, 1995

Effects of Correlated Noise on the Full-Spectrum Combining and Complex-Symbol Combining Arraying Techniques

P. Vazirani
Communications Systems Research Section

The process of combining telemetry signals received at multiple antennas, commonly referred to as arraying, can be used to improve communication link performance in the Deep Space Network (DSN). By coherently adding telemetry from multiple receiving sites, arraying produces an enhancement in signal-to-noise ratio (SNR) over that achievable with any single antenna in the array. A number of different techniques for arraying have been proposed and their performances analyzed in past literature [1,2]. These analyses have compared different arraying schemes under the assumption that the signals contain additive white Gaussian noise (AWGN) and that the noise observed at distinct antennas is independent.

In situations where an unwanted background body is visible to multiple antennas in the array, however, the assumption of independent noises is no longer applicable. A planet with significant radiation emissions in the frequency band of interest can be one such source of correlated noise. For example, during much of Galileo's tour of Jupiter, the planet will contribute significantly to the total system noise at various ground stations. This article analyzes the effects of correlated noise on two arraying schemes currently being considered for DSN applications: full-spectrum combining (FSC) and complex-symbol combining (CSC). A framework is presented for characterizing the correlated noise based on physical parameters, and the impact of the noise correlation on the array performance is assessed for each scheme.

I. Introduction

Arraying spacecraft telemetry has a number of desirable applications in the Deep Space Network. By combining signals from multiple antennas, arraying has the benefit of increasing the signal-to-noise ratio (SNR) of the combined signal over that achievable with any individual antenna in the array. Arraying may be used to coherently track signals that are too weak to be tracked by a single antenna or to allow an increase in the supportable data rate for stronger signals. Several different schemes for performing arraying have been proposed and analyzed in past literature [1,2]. These schemes differ in the synchronization processes that are used to combine and demodulate the signals. Thus, a benchmark used to compare different arraying schemes is symbol SNR degradation, which is a measure of the SNR reduction due to imperfect synchronization for a particular scheme.

Previous analyses that have compared arraying techniques in terms of symbol SNR degradation have used an additive white Gaussian noise (AWGN) model to describe the deep-space channel and have assumed the noise waveforms received at distinct antennas are independent. However, if a strong radio source is within the antenna pattern of multiple antennas in the array, the noise observations at different antennas become correlated. For a substantial fraction of Galileo's encounter with Jupiter, for example, the planet will have an angular separation from the spacecraft that is less than the beamwidth of a 70-m antenna at S-band (2.3 GHz).[1] Further analysis is thus needed to characterize the performance of arraying schemes in cases where correlated noise is present.

Prior work has been conducted on this subject but has not exhausted research possibilities. A study by Dewey [3] examines correlated noise effects due to planetary sources, focusing mainly on physical considerations. A correlated noise model is presented, taking into account properties of the source and the array geometry. The impact of the background source on arrayed symbol SNR relative to a case of uncorrelated noise is then analyzed. The results obtained are applied to observation of the Galileo spacecraft from a four-element array in the DSN's Australia complex. However, Dewey's study does not take into account the effects of imperfect synchronization in telemetry arraying, which are dependent on the specific arraying technique used. Thus, the analysis does not identify the relative advantages and disadvantages of different arraying schemes under conditions of correlated noise.

The purpose of this article is to analyze the effects of correlated noise on the full-spectrum combining (FSC) and complex-symbol combining (CSC) arraying schemes. In Section II, background material needed to understand the physics underlying background noise in receiving systems is presented. Parameters used to characterize the noise correlation properties will be introduced and explained. Sections III and IV then apply this model to the FSC and CSC techniques and compute the symbol SNR degradation for each scheme. Section V applies the results of the previous sections to the Galileo mission. Predicts for the signal and noise parameters are used to evaluate the performance of both arraying schemes in this scenario. Finally, Section VI summarizes the main results of the work.

II. Background Noise Properties

Here we present basic terminology used to describe broadband sources that will be used for the remainder of the analysis. The discussion that follows is included only to summarize major results from previous work; readers interested in a more thorough treatment of the subject material may refer to a text on radio astronomy, such as [4], or the work performed by Dewey alluded to earlier [3].

Consider first the effect of a background source on a single receiving system. The noise observed at an antenna consists of both thermal noise due to front-end receiver electronics and radiation due to any radio sources in the antenna's field of view. Such sources typically have an emission spectrum that varies very slowly with frequency and can, therefore, be considered white over the bandwidth of interest.[2] The increase in total system temperature due to the background source is found by integrating the source's brightness distribution over the antenna's reception pattern, i.e.,

$$T_s = \frac{A_e}{2k} \int \int B(\hat{s}) P_N(\hat{s})\, d\hat{s} \tag{1}$$

where A_e is the effective receiving area of the antenna in m^2; k is Boltzmann's constant, 1.379×10^{-23} W/K/Hz; $B(\hat{s})$ is the brightness of the source in $W/m^2/Hz/sr$ (sr stands for steradian, a measure of solid angle); $P_N(\hat{s})$ is the normalized antenna reception pattern; and $\hat{s}$ is a unit vector specifying direction.

[1] G. Resch, "Jupiter's Contribution to the Total System Temperature at S-Band During the Galileo Mission," JPL Interoffice Memorandum 335.3-92.02 (internal document), Jet Propulsion Laboratory, Pasadena, California, June 23, 1993.

[2] Ibid.

The one-sided power spectral density of the noise due to the source is then given by $N_s = kT_s$. Note that in the upper limit, when the source is concentrated in the peak of the antenna's reception pattern, the temperature increase is given by

$$T_s = \frac{A_e}{2k} \int\int B(\hat{s})\, d\hat{s} \tag{2}$$

$$= \frac{A_e}{2k} S \tag{3}$$

where S is the total flux density of the source in $W/m^2/Hz$. As the angular separation between the source and the spacecraft increases, the background source moves out of the peak of the antenna pattern, and its temperature contribution diminishes. In addition, the flux density for a particular source is dependent on its distance to Earth; the greater the range, the smaller the observed flux is. Thus, the temperature contribution for a body depends on both its strength and its position.

Now consider a pair of antennas physically separated by a baseline vector $\vec{B}_{ik}$ observing a common source. The cross-correlation function for the baseband (BB) noise processes $\tilde{n}_i(t)$ and $\tilde{n}_k(t)$ can be written as

$$R_{\tilde{n}_i,\tilde{n}_k}(\tau) \triangleq E[\tilde{n}_i(t)\tilde{n}_k^*(t-\tau)] = \alpha\, \frac{\sin(2\pi B\tau)}{\pi\tau} \tag{4}$$

where B is the one-sided bandwidth of the noise waveforms, and α is their cross-power spectral density. If the bandwidth B is wider than the telemetry bandwidth, then the cross-spectrum is white over the bandwidth of interest, and the "sinc" function $\sin(2\pi B\tau)/(\pi\tau)$ can be approximated by an impulse function, i.e.,

$$R_{\tilde{n}_i,\tilde{n}_k}(\tau) = \alpha\, \delta(\tau) \tag{5}$$

It can be shown [3,4] that the cross-power spectral density level is given by

$$\alpha = \frac{\sqrt{A_{e_i} A_{e_k}}}{2} \int\int B(\hat{s}) \sqrt{P_{N_i}(\hat{s}) P_{N_k}(\hat{s})}\, e^{j2\pi f_o \vec{B}_{ik}\cdot\hat{s}/c}\, d\hat{s}$$

$$= \frac{\sqrt{A_{e_i} A_{e_k}}}{2} |V| e^{j\phi_v} \tag{6}$$

where f_o is the observation frequency, and c is the speed of light, 3×10^8 m/s. In radio interferometry applications, the quantity $|V|e^{j\phi_v}$ is known as the complex visibility of the source. A few important observations regarding Eq. (6) are made here. First, note that the exponential term $e^{j2\pi f_o \vec{B}_{ik}\cdot\hat{s}/c}$ produces a sinusoidal variation over the spatial extent of the source. This variation is known as the fringe pattern formed by a particular pair of antennas. The period of these fringe oscillations is given in radians/cycle by $c/f_o B_{ik_p}$, where B_{ik_p} is the projected baseline length in the direction of the source. If a source has an angular size much greater than the fringe period, the cross-correlation magnitude then tends to zero due to the averaging effect of the sinusoid. Thus, in the long baseline limit (i.e., $B_{ik_p} \gg c/(f_o R_s)$, with R_s being the angular radius of the source), $|\alpha| \to 0$, and the noise observations due to the source become uncorrelated. By contrast, for $B_{ik_p} \ll c/(f_o R_s)$, the magnitude of the cross-power spectral density achieves its upper limit, namely

$$|\alpha| \rightarrow \frac{\sqrt{A_{e_i} A_{e_k}}}{2} S \tag{7}$$

Thus, the degree of noise correlation observed by an array of antennas depends heavily on the geometry of the array. This point is stressed in [3], where it is stated that the more compact the array configuration, the greater the impact of a background body on the array.

Finally, we introduce the correlation coefficient, describing the degree of correlation that exists between the noise at two antennas, defined as

$$\rho_{ik} \triangleq \frac{|\alpha|}{\sqrt{N_{o_i} N_{o_k}}} \tag{8}$$

Note that in the upper limit (i.e., source size small compared to fringe period), the correlation coefficient becomes

$$\rho_{ik} \rightarrow \sqrt{\frac{T_{s_i} T_{s_k}}{T_i T_k}} \tag{9}$$

where T_{s_i}, T_{s_k} are the source temperatures at antennas i, k, and T_i, T_k are the *total* system temperatures at the two antennas. Thus, the greater the contribution of the source to the total system temperature, the higher the correlation coefficient, as is intuitively expected.

Combining Eqs. (5), (6), and (8), the cross-correlation function for the noise observed at two antennas can be expressed as

$$R_{\tilde{n}_i, \tilde{n}_k}(\tau) = \rho_{ik} \sqrt{N_{o_i} N_{o_k}}\ e^{j\phi^n_{ik}}\ \delta(\tau) \tag{10}$$

where ϕ^n_{ik} is used to express the correlation phase, denoted by ϕ_v in Eq. (6).

III. Full-Spectrum Combining Performance

Given a mathematical description of noise correlation properties, we now apply the model to analyzing correlated noise effects on arraying. Full-spectrum combining is described in detail in [2] and summarized here briefly. Assume the array consists of L antennas, where antenna 1 is taken to be the "master" antenna (i.e., the antenna with the highest G/T.) As shown in Fig. 1, each signal is first downconverted to baseband[3] by local oscillators in phase quadrature. Each signal pair, which can be thought of as a single complex signal, is then shifted in time by some amount $\hat{\tau}_i$ to compensate for differing arrival times of the spacecraft signal at the various antennas. The complex baseband signals are then aligned in phase, multiplied by prespecified weighting factors, and added. Finally, the combined signal is processed by a single carrier, subcarrier, and symbol loop.

Two quantities used to describe arraying performance are the ideal arraying gain, denoted by G_A, and the symbol SNR degradation, denoted by D. The arraying gain is defined as the ratio of the ideal symbol SNR of the arrayed signal to the ideal symbol SNR of antenna 1 [1]. Here, "ideal" means the

[3] Analysis presented in [2] actually assumes all processing is done at an intermediate frequency, rather than at baseband. A baseband system was assumed here to simplify the analysis. This represents no loss of generality, since final results are not dependent on what frequency processing is done at.

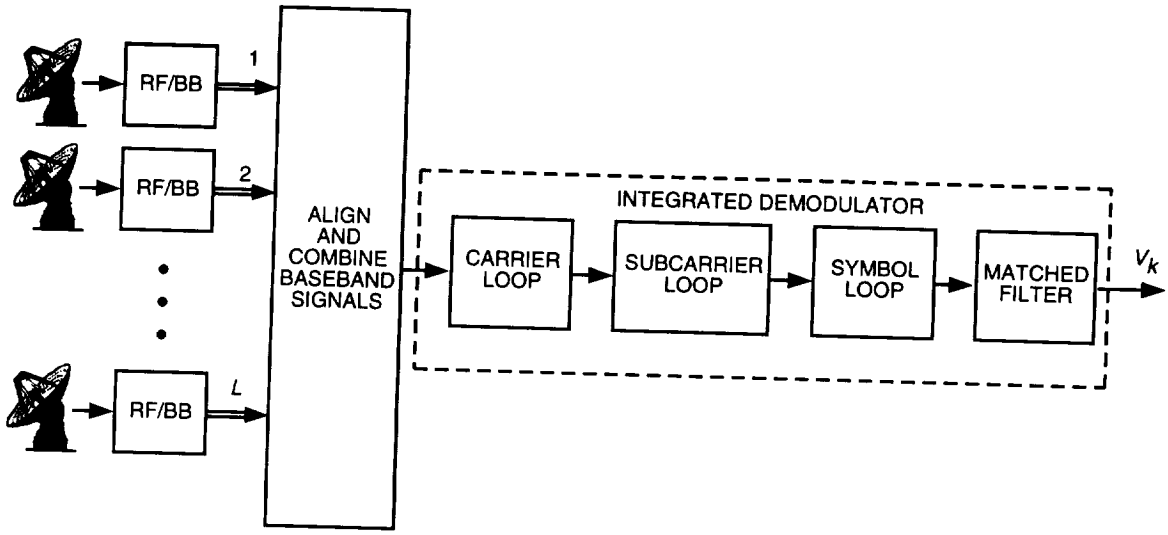

Fig. 1. Full-spectrum combining.

symbol SNR that would be achieved in the absence of synchronization errors (i.e., perfect signal combining and perfect carrier, subcarrier, and symbol references.) Note that the arraying gain G_A is *independent* of which arraying technique is used, since synchronization losses are ignored. Thus, G_A describes the maximum SNR enhancement that can be achieved by arraying, but is not useful for evaluating the relative performance of one arraying scheme over another. The ideal arraying gain is computed in [1] for a set of antennas observing independent noise waveforms. Our first step in evaluating the impact of a background body on arraying will be to compute G_A for the case of correlated noise. This analysis is analogous to that found in [3], although the notation adopted here is different.

Degradation is defined as the ratio of the actual SNR of the arrayed telemetry to that achieved with perfect synchronization (i.e., the ideal SNR). Clearly, degradation is dependent on which arraying scheme is used, since synchronization losses depend on the specific processing used to combine and demodulate the signals. Degradation for full-spectrum combining and complex-symbol combining was computed in [2], also under the assumption of independent noises. Thus, the second step in analyzing correlated noise effects will be to derive degradation expressions for the two schemes.

A. Ideal Arraying Gain

The signal format for deep-space telemetry is binary phase shift keyed (BPSK) employing a squarewave subcarrier. After time alignment, the IF signal from the ith antenna can be expressed as [1]

$$\begin{aligned} y_i(t) &= s_i(t) + n_i(t) \\ &= \sqrt{2P_{T_i}} \cos\left(\omega_{IF}t + \theta_i + \Delta d(t)\ \mathrm{sqr}(\omega_{sc}t + \theta_{sc})\right) + n_i(t) \\ &= \sqrt{2P_{C_i}} \cos\left(\omega_{IF}t + \theta_i\right) - \sqrt{2P_{D_i}} d(t)\ \mathrm{sqr}(\omega_{sc}t + \theta_{sc}) \sin(\omega_{IF}t + \theta_i) + n_i(t) \end{aligned} \tag{11}$$

where P_{T_i} is the total signal power in watts; ω_{IF} is the intermediate frequency in radians/s; θ_i is the carrier phase in radians; Δ is the modulation index in radians; $d(t)$ is the binary data, taking on values of ± 1; $\mathrm{sqr}(x)$ is the squarewave function, given by $\mathrm{sqr}(x) = \mathrm{sgn}(\sin x)$; ω_{sc} is the subcarrier frequency in radians/s; θ_{sc} is the subcarrier phase in radians; P_{C_i} is the carrier power in watts, given by $P_{C_i} = P_{T_i} \cos^2 \Delta$; P_{D_i} is the data power in watts, given by $P_{D_i} = P_{T_i} \sin^2 \Delta$; and $n_i(t)$ is an additive white

Gaussian noise process with one-sided power spectral density N_{o_i} W/Hz. The corresponding complex baseband signal is given by

$$\tilde{y}_i(t) = \tilde{s}_i(t) + \tilde{n}_i(t) \tag{12}$$

$$= \sqrt{P_{C_i}} e^{j(\omega_b t + \theta_i)} + j\sqrt{P_{D_i}} d(t)\ \mathrm{sqr}(\omega_{sc} t + \theta_{sc}) e^{j(\omega_b t + \theta_i)} + \tilde{n}_i(t) \tag{13}$$

where ω_b is the baseband frequency (which, by definition, is close to zero), and $\tilde{n}_i(t)$ is the complex baseband noise, the real and imaginary parts of which each has one-sided power spectral density N_{o_i}. The spectrum of the baseband telemetry is shown in Fig. 2.

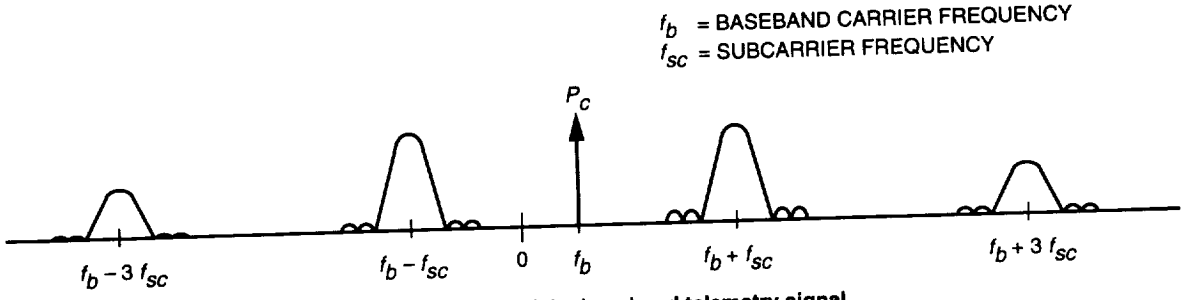

Fig. 2. Spectrum of the baseband telemetry signal.

Note that the bandwidth needed to transmit the signals $\tilde{y}_i(t)$ to a common location for combining is determined by the subcarrier frequency, $f_{sc} = \omega_{sc}/2\pi$, and is much greater than the actual data rate. As an alternative to the method described in [2], a version of FSC that only transmits portions of the spectrum containing signal energy can be used to reduce this bandwidth requirement. Each signal can be passed through a bank of matched filters separately, passing the subcarrier harmonics with the data modulation; the total transmission bandwidth is then proportional to the data rate. This alternative is mentioned briefly in [1]. However, the drawback of such a system is that the processing required is dependent on the subcarrier frequency and data rate and must be modified for each mission. For simplicity, we will focus on the more basic implementation of FSC described in [2], keeping in mind that a more bandwidth-economizing option also exists.

Let the phase difference between the 1st and ith signal be denoted by $\phi_{1i} = \theta_1 - \theta_i$. In the algorithm described in [1], signals 2 through L are phase rotated by an estimate of this quantity, $\hat{\phi}_{1i}$, to align them with signal 1. The aligned signals are then multiplied by prespecified weighting factors, β_i, and summed. The combined signal is thus given by

$$\tilde{y}_{comb}(t) = \tilde{s}_{comb}(t) + \tilde{n}_{comb}(t) \tag{14}$$

$$= \sum_{i=1}^{L} \beta_i e^{j\hat{\phi}_{1i}} \tilde{s}_i(t) + \sum_{i=1}^{L} \beta_i e^{j\hat{\phi}_{1i}} \tilde{n}_i(t) \tag{15}$$

$$= \sum_{i=1}^{L} \beta_i e^{j\hat{\phi}_{1i}} \left(\sqrt{P_{C_i}} e^{j(\omega_b t + \theta_i)} + j\sqrt{P_{D_i}} d(t)\ \mathrm{sqr}(\omega_{sc} t + \theta_{sc}) e^{j(\omega_b t + \theta_i)} \right)$$

$$+ \sum_{i=1}^{L} \beta_i e^{j\hat{\phi}_{1i}} \tilde{n}_i(t) \tag{16}$$

where the weights β_i are chosen to satisfy the condition

$$\beta_i = \sqrt{\frac{P_{T_i}}{P_{T_1}}} \frac{N_{o1}}{N_{oi}} \tag{17}$$

for $i = 1, \cdots, L$. It is shown in [1] that these weights maximize the combined SNR when the noises $\tilde{n}_i(t)$ are independent. Note that this is *not* necessarily the optimal choice of weights for the correlated noise case, as pointed out in [3]. Furthermore, the optimal choice of phases used to array the signals is not necessarily the relative signal phases, ϕ_{1i}. Using the phases ϕ_{1i} will certainly maximize the arrayed signal power, but not necessarily the *ratio* of signal to noise power, which is the relevant criteria for optimization. The problem of optimal combining weights and phases for signals with correlated noise has been analyzed in [5], where the results are applied to an array of antenna feed elements. However, computation of these weights requires knowledge of the pairwise correlations between the noises, $\alpha_{ij}e^{j\phi^n_{ij}}$, for all i, j pairs. A scheme can be devised to estimate the required parameters in real time and modify the weights accordingly, but would significantly complicate the problem. Our goal, instead, is to determine the performance impact of the correlated noise assuming the traditional combining scheme is used.

The total combined signal power, P_T, is given by

$$P_T \triangleq E\left[\tilde{s}_{comb}(t)\right] \; E\left[\tilde{s}^*_{comb}(t)\right] \tag{18}$$

If the relative signal phases are estimated perfectly (i.e., $\hat{\phi}_{1i} = \phi_{1i}$ for $i = 2, \cdots, L$), the combined signal power becomes

$$P_T = P_{T_1}\left(\sum_{i=1}^{L}\gamma_i^2 + \sum_{i=1}^{L}\sum_{\substack{j=1 \\ i\neq j}}^{L}\gamma_i\gamma_j\right) \tag{19}$$

where $\gamma_i \triangleq [(P_{T_i})/(P_{T_1})][(N_{o_1})/(N_{o_i})]$.

The one-sided power spectral density of the real and imaginary parts of the combined noise is given by

$$N_o \triangleq \frac{1}{2B}E\left[\tilde{n}_{comb}(t)\; \tilde{n}^*_{comb}(t)\right] \tag{20}$$

where B is the one-sided bandwidth of the noise waveforms. Note that the factor of two in the denominator of Eq. (20) results from the fact that the real and imaginary parts of the noise each has half the power of the complex noise. From the definitions of power spectral density and cross-power spectral density, it follows that

$$E\left[\tilde{n}_i(t)\tilde{n}^*_i(t)\right] \; = 2N_{o_i}B \tag{21}$$

$$E\left[\tilde{n}_i(t)\tilde{n}^*_j(t)\right] \; = 2\alpha_{ij}e^{j\phi^n_{ij}}B \tag{22}$$

Equations (20), (21), and (22) can be combined to find the power spectral density of the combined noise, yielding

$$N_o = N_{o_1}\left(\sum_{i=1}^{L}\gamma_i + \sum_{i=1}^{L}\sum_{\substack{j=1\\ i\neq j}}^{L}\sqrt{\gamma_i\gamma_j}\rho_{ij}e^{j(\phi_{ij}^n-\phi_{ij})}\right) \tag{23}$$

The P_T/N_o of the combined signal is thus given by

$$\frac{P_T}{N_o} = \frac{P_{T_1}}{N_{o_1}}\frac{\left(\sum_{i=1}^{L}\gamma_i\right)^2}{\sum_{i=1}^{L}\gamma_i + \sum_{i=1}^{L}\sum_{\substack{j=1\\ i\neq j}}^{L}\sqrt{\gamma_i\gamma_j}\ \rho_{ij}\ e^{j\psi_{ij}}} \tag{24}$$

where $\psi_{ij} \triangleq \phi_{ij}^n - \phi_{ij}$. The parameters ρ_{ij} and ψ_{ij} describe the relevant statistics for the noise correlations between the various antenna pairs and determine the correlated noise impact on the ideal arraying gain.

The combined signal is finally processed by a single carrier, subcarrier, and symbol loop. Assuming perfect references at each of these three stages, the symbol SNR of the arrayed signal becomes

$$\begin{aligned} SNR_{ideal} &= \frac{2P_{D_1}}{N_{o_1}R_{sym}}\frac{(\sum_{i=1}^{L}\gamma_i)^2}{\sum_{i=1}^{L}\gamma_i + \sum_{i=1}^{L}\sum_{\substack{j=1\\ i\neq j}}^{L}(\gamma_i\gamma_j)^{1/2}\rho_{ij}\ e^{j\psi_{ij}}} \\ &= \frac{2P_{D_1}}{N_{o_1}R_{sym}}\ G_A \end{aligned} \tag{25}$$

where G_A is the ideal arraying gain due to combining the signals. Note that setting all the noise correlation coefficients ρ_{ij} to zero results in $G_A = \sum_{i=1}^{L}\gamma_i$, which is the ideal arraying gain in the case of uncorrelated noises, as discussed in [1].

Further note that the ideal arraying gain in the presence of correlated noise can be higher *or* lower than the uncorrelated noise case, depending on the phases ψ_{ij}. This point can be understood by considering an array of two equal antennas (i.e., $\gamma_1 = \gamma_2 = 1$.) Figure 3 shows values for G_A for two equal antennas as a function of ρ and ψ. For $\rho = 0$, the ideal arraying gain is a constant 3 dB, as expected. Now suppose the noises have some nonzero correlation coefficient, ρ, and some correlation phase, ϕ^n. If $\psi = 0$ deg, then the phase difference of the spacecraft signal as observed by antennas 1 and 2, ϕ, is equal to the noise correlation phase ϕ^n. Thus, phase aligning the two signals *also* phase aligns the correlated component of the noise. The noise from the background source adds maximally in phase, and the combined noise power increases. Thus, the combined SNR decreases, and hence the arraying gain falls below 3 dB. By contrast, if $\psi = 180$ deg, phase aligning the signal results in combining the correlated component of the noise 180 deg out of phase. Thus, the noise combines destructively in this case, and the arraying gain is now *greater* than 3 dB. For intermediate values of ψ, the arraying gain varies continuously from its minimum value at $\psi = 0$ deg to its maximum at $\psi = 180$ deg.

B. Symbol SNR Degradation

In practice, perfect phase alignment and ideal carrier, subcarrier, and symbol references are not available. Some degradation in the arrayed symbol SNR is, therefore, incurred due to synchronization errors. To quantify the degradation, we first find the set of density functions for the phase alignment errors $\Delta\phi_{1i} \triangleq \hat{\phi}_{1i} - \phi_{1i}$, $i = 2, \cdots, L$. This set of functions is then used to compute the P_T/N_o of the arrayed signal. Adding in losses due to carrier, subcarrier, and symbol tracking, the symbol SNR at the matched-filter output can be computed. Finally, comparing the actual symbol SNR to the ideal symbol SNR given by Eq. (25) yields the degradation for full-spectrum combining.

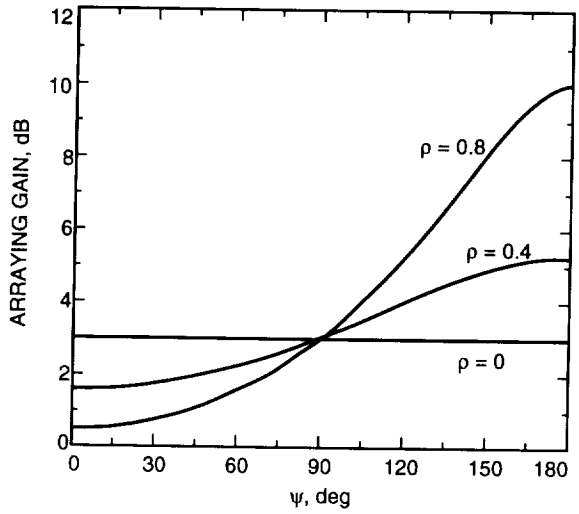

Fig. 3. Ideal arraying gain G_A for various ρ,ψ.

1. Antenna Phasing. A set of phase estimates $\hat{\phi}_{1i}$ for $i = 2, \cdots, L$ are needed to align signals $2, \cdots, L$ with signal 1. In the description of FSC given in [2], the phase difference between $\tilde{s}_i(t)$ and $\tilde{s}_1(t)$ is estimated by filtering the two signals to some lowpass bandwidth B_{lp} Hz, multiplying them, and averaging their product over T_{corr} s. The phase of this complex quantity is then computed by taking the inverse tangent of the ratio of the imaginary to real parts. A block diagram of this scheme is shown in Fig. 4.

The complex product of the baseband signals after averaging, Z, is given by

$$Z = \frac{1}{T_{corr}} \int (\tilde{s}_{lp_1}(t) + \tilde{n}_{lp_1}(t))(\tilde{s}^*_{lp_i}(t) + \tilde{n}^*_{lp_i}(t))\, dt$$

$$= (\sqrt{P_{C_1} P_{C_i}} + \sqrt{P_{D_1} P_{D_i}} H) e^{j\phi_{1i}} + \frac{1}{T_{corr}} \int \left(\tilde{n}_{s,n}(t) + \tilde{n}_{lp_1}(t)\tilde{n}^*_{lp_i}(t)\right)\, dt \tag{26}$$

where H is given by

$$H = \left(\frac{4}{\pi}\right)^2 \sum_{\substack{i=1 \\ i \text{ odd}}}^{M} \frac{1}{2i^2} \tag{27}$$

and M is the highest harmonic of the subcarrier passed by the lowpass filter. The term $\tilde{n}_{s,n}(t)$ is composed of signal-noise terms in the product and has zero mean. Note, however, that the noise-noise term, $\tilde{n}_{lp_1}(t)\tilde{n}_{lp_i}(t)^*$, does not necessarily have zero mean, due to a possible correlation that exists between the two noise waveforms. The expected value of this noise product can easily be computed from the cross-power spectral density of $\tilde{n}_1(t)$ and $\tilde{n}_i(t)$; thus,

$$E[z] = (\sqrt{P_{C_1} P_{C_i}} + \sqrt{P_{D_1} P_{D_i}} H) e^{j\phi_{1i}} + 2\rho_{1,i} \sqrt{N_{o_1} N_{o_i}} B_{lp} e^{j\phi^n_{1i}} \tag{28}$$

Since ϕ^n_{1i} is not necessarily equal to ϕ_{1i}, the noise product introduces a "bias" to the estimate of the relative signal phase. This situation is represented pictorially in Fig. 5. The complex quantity $E[z]$ can

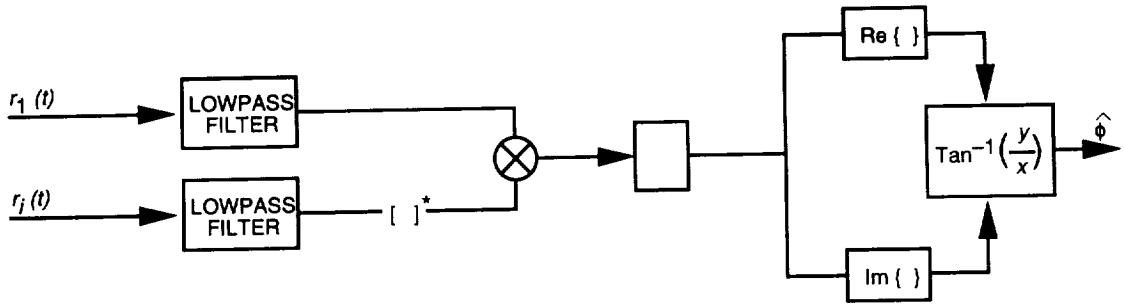

Fig. 4. Conventional phase estimator.

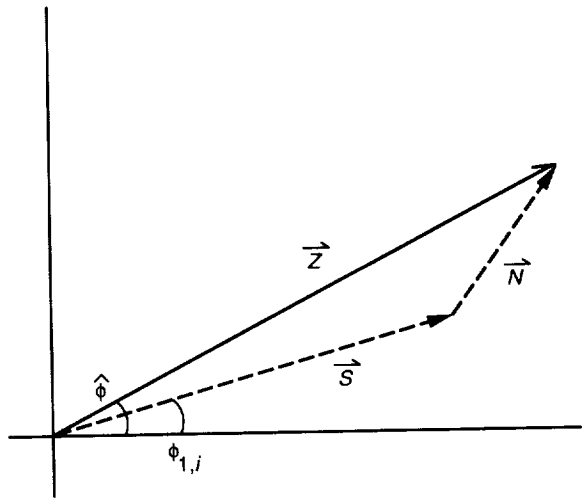

Fig. 5. Complex correlation vector.

be thought of as a vector sum of a signal-to-signal correlation, $\vec{S}$, and a noise-to-noise correlation, $\vec{N}$. Note how the presence of the noise vector biases the measurement of the phase of the complex correlation. The relative magnitude of these vectors is given by

$$\frac{|\vec{S}|}{|\vec{N}|} = \frac{1}{2\rho_{1i}\, B_{lp}} \left(\left(\frac{P_{C_1}}{N_{o_1}} \frac{P_{C_i}}{N_{o_i}} \right)^{1/2} + H \left(\frac{P_{D_1}}{N_{o_1}} \frac{P_{D_i}}{N_{o_i}} \right)^{1/2} \right) \tag{29}$$

For typical parameters, even relatively modest levels of noise correlation can lead to a substantial biasing effect in estimating the relative signal phase. For example, consider correlating two signals, each having a P_T/N_o of 20 dB-Hz with a 1-kHz correlation bandwidth. Even if all subcarrier harmonics are included in the correlation, making $H = 1$, a correlation coefficient as low as $\rho = 0.1$ makes the ratio in Eq. (29) equal to 0.5. The phase estimates are then influenced more by the relative *noise* phases ϕ_{1i}^n than the desired quantities ϕ_{1i}, leading to a high amount of degradation in combining the signals. If the alternative method described in Section III.A is used, where the subcarrier harmonics are filtered individually prior to combining, the effective correlation bandwidth can be lessened, thus reducing the impact of the noise bias. Nevertheless, a practical implementation of full-spectrum combining requires a modified phase estimation algorithm if correlation levels encountered will generate significant biases.

The method of phase estimation shown in Fig. 6 can be used for this purpose. Here, each signal is filtered to some bandpass bandwidth B_{bp}, and an additional complex correlation is performed between

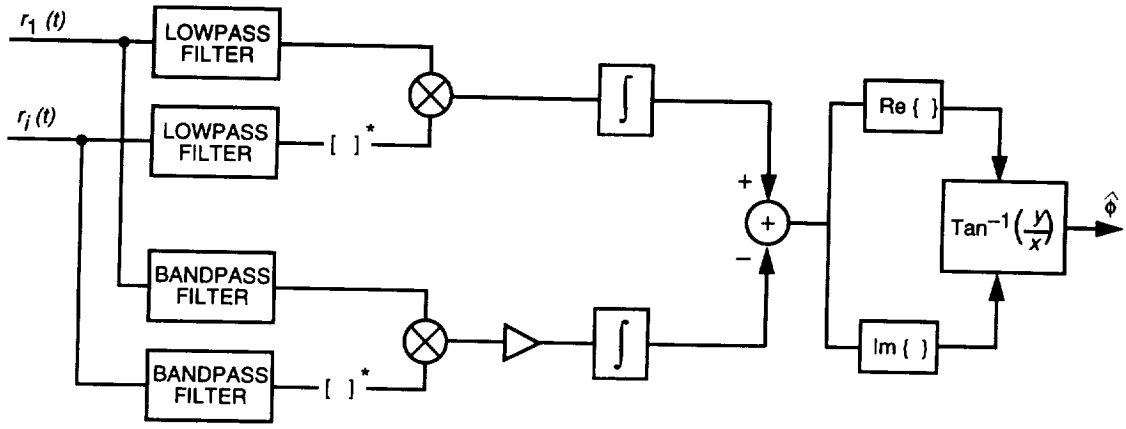

Fig. 6. Modified phase estimator.

the resulting waveforms. The center frequency of this filter is chosen so as to *not* capture any energy from the telemetry; this can be accomplished by locating the filter at an even multiple of the subcarrier frequency, for example. After scaling the noise-only correlation by the ratio of the lowpass-to-bandpass bandwidths, this quantity provides an estimate of the contribution of the noise to the total correlation. The bandpass correlation can then be subtracted from the lowpass correlation to compensate for the mean correlation vector $|\vec{N}|$. The compensated correlation can thus be expressed as

$$\begin{aligned} Z &= \left(\sqrt{P_{C_1}P_{C_i}} + \sqrt{P_{D_1}P_{D_i}}H\right)e^{j\phi_{1i}} + \frac{1}{T_{corr}}\int \left(\tilde{n}_{s,n}(t) + \tilde{n}_{lp_1}(t)\tilde{n}^*_{lp_i}(t)\right)\, dt \\ &\quad - \frac{B_{lp}}{B_{bp}}\frac{1}{T_{corr}}\int \tilde{n}_{bp_1}(t)\tilde{n}^*_{bp_i}(t)\, dt \\ &= (\sqrt{P_{C_1}P_{C_i}} + \sqrt{P_{D_1}P_{D_i}}H)e^{j\phi_{1i}} + \tilde{N} \end{aligned} \tag{30}$$

where the the noise term $\tilde{N}$ now has zero mean. The phase estimate is then found by taking the inverse tangent of the ratio of the imaginary-to-real part of Eq. (30), i.e.,

$$\hat{\phi}_{1i} = \tan^{-1}\left[\frac{(\sqrt{P_{C_1}P_{C_i}} + \sqrt{P_{D_1}P_{D_i}}H)\sin\phi_{1i} + N_Q}{(\sqrt{P_{C_1}P_{C_i}} + \sqrt{P_{D_1}P_{D_i}}H)\cos\phi_{1i} + N_I}\right] \tag{31}$$

where N_I and N_Q are the real and imaginary parts of $\tilde{N}$, respectively. Note that although N_I and N_Q have zero mean, their joint statistics are *still* influenced by the correlation between $\tilde{n}_1(t)$ and $\tilde{n}_i(t)$. These statistics are analyzed in Appendix A, and the density function for the phase estimation error $\Delta\phi_{1i} \triangleq \hat{\phi}_{1i} - \phi_{1i}$ is derived.

In [2], a quantity known as the *correlator SNR* is introduced, defined as

$$SNR_{corr} = \frac{E[Z]E^*[Z]}{E[ZZ^*] - E[Z]E^*[Z]} \tag{32}$$

The correlator SNR is a measure of the spread of the phase error density $p_\phi(\Delta\phi_{1i})$ and is inversely related to the variance of the phase error. In [1], where FSC is analyzed for independent noises, it is shown that

the phase error density can be expressed solely in terms of the correlator SNR. For the correlated noise case, the density is given in Appendix A in terms of the correlator SNR and the correlation parameters ρ_{1i} and ψ_{1i}.

Figures 7 through 9 show the density function $p_\phi(\Delta\phi)$ for various values of ρ and ψ. The signal parameters chosen for these curves are $(P_T/N_o)_1 = (P_T/N_o)_2 = 25$ dB-Hz, $\Delta = 90$ deg, with seven subcarrier harmonics included in the correlation. The correlator parameters are $B_{lp} = B_{bp} = 15$ kHz, and $T_{corr} = 3$ s. Note that even for a noise correlation as high as 0.4, the density function looks remarkably like that of the uncorrelated noise case. Simulations were performed for the same parameters and densities collected for the measured phase estimates. These results are shown with the analytical curves in Fig. 10.

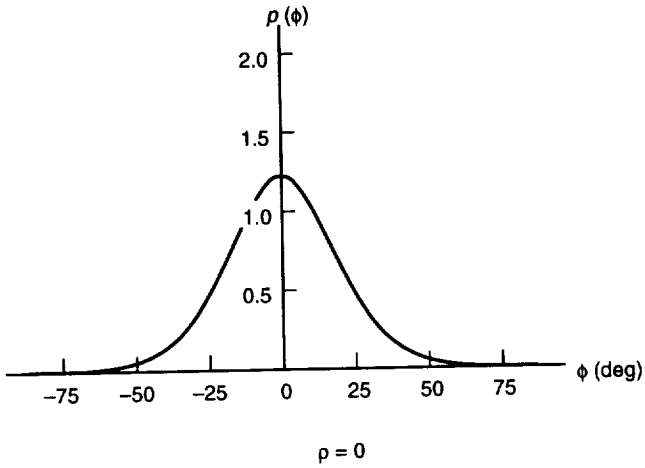

Fig. 7. Phase estimate density.

2. Arrayed Symbol SNR and Symbol SNR Degradation. Using the set of estimated phases to align the signals, the combined signal becomes

$$\tilde{y}_{comb}(t) = \tilde{s}_{comb}(t) + \tilde{n}_{comb}(t) \tag{33}$$

$$= \sum_{i=1}^{L} \beta_i \, e^{j\hat{\phi}_{1i}} \tilde{s}_i(t) + \sum_{i=1}^{L} \beta_i \, e^{j\hat{\phi}_{1i}} \tilde{n}_i(t) \tag{34}$$

$$= \sum_{i=1}^{L} \beta_i \left(\sqrt{P_{C_i}} - j\sqrt{P_{D_i}} \, \mathrm{sqr}(\omega_{sc}t + \theta_{sc}) \right) e^{j(\omega_b t + \theta_1 + \Delta\phi_{1i})} + \sum_{i=1}^{L} \beta_i e^{j\hat{\phi}_{1i}} \tilde{n}_i(t) \tag{35}$$

The combined signal power conditioned on the set of phase errors $\Delta\phi_{1i}$ is thus given by

$$P'_T = E\left[\tilde{s}_{comb}(t)\right] E\left[\tilde{s}^*_{comb}(t)\right] \tag{36}$$

$$= P_{T_1} \left(\sum_{i=1}^{L} \gamma_i^2 + \sum_{i=1}^{L} \sum_{\substack{j=1 \\ i \neq j}}^{L} \gamma_i \gamma_j e^{j(\Delta\phi_{1i} - \Delta\phi_{1j})} \right) \tag{37}$$

Similarly, the conditional noise power spectral density is given by

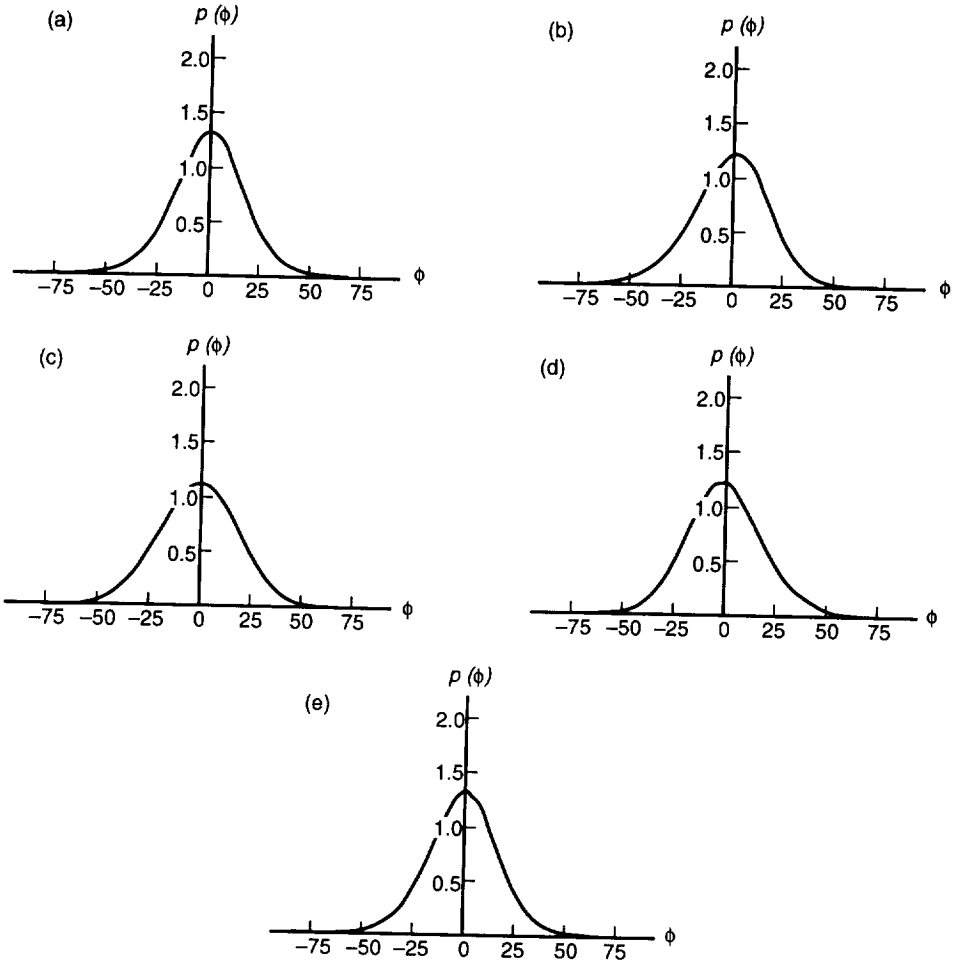

Fig. 8. Phase estimate densities: (a) $\rho = 0.4$, $\Psi = 0$ deg, (b) $\rho = 0.4$, $\Psi = 45$ deg, (c) $\rho = 0.4$, $\Psi = 90$ deg, (d) $\rho = 0.4$, $\Psi = 135$ deg, and (e) $\rho = 0.4$, $\Psi = 180$ deg.

$$N_o' = \frac{1}{2B} E\left[\tilde{n}_{comb}(t)\tilde{n}^*_{comb}(t)\right] \tag{38}$$

$$= N_{o_1}\left(\sum_{i=1}^{L}\gamma_i + \sum_{i=1}^{L}\sum_{\substack{j=1\\ i\neq j}}^{L}(\gamma_i\gamma_j)^{1/2}\rho_{ij}\, e^{j\psi_{ij}}\, e^{j(\Delta\phi_{1i}-\Delta\phi_{1j})}\right) \tag{39}$$

Taking the ratio of Eq. (37) to Eq. (39) yields the conditional P_T/N_o of the combined signal, i.e.,

$$\left(\frac{P_T}{N_o}\right)' = \frac{P_{T1}}{N_{o1}} \frac{\sum_{i=1}^{L}\gamma_i^2 + \sum_{i=1}^{L}\sum_{\substack{j=1\\ i\neq j}}^{L}\gamma_i\gamma_j e^{j(\Delta\phi_{1i}-\Delta\phi_{1j})}}{\sum_{i=1}^{L}\gamma_i + \sum_{i=1}^{L}\sum_{\substack{j=1\\ i\neq j}}^{L}(\gamma_i\gamma_j)^{1/2}\,\rho_{ij}\, e^{j\psi_{ij}}\, e^{j(\Delta\phi_{1i}-\Delta\phi_{1j})}} \tag{40}$$

After carrier and subcarrier demodulation and matched filtering, the conditional symbol SNR of the arrayed signal is given by

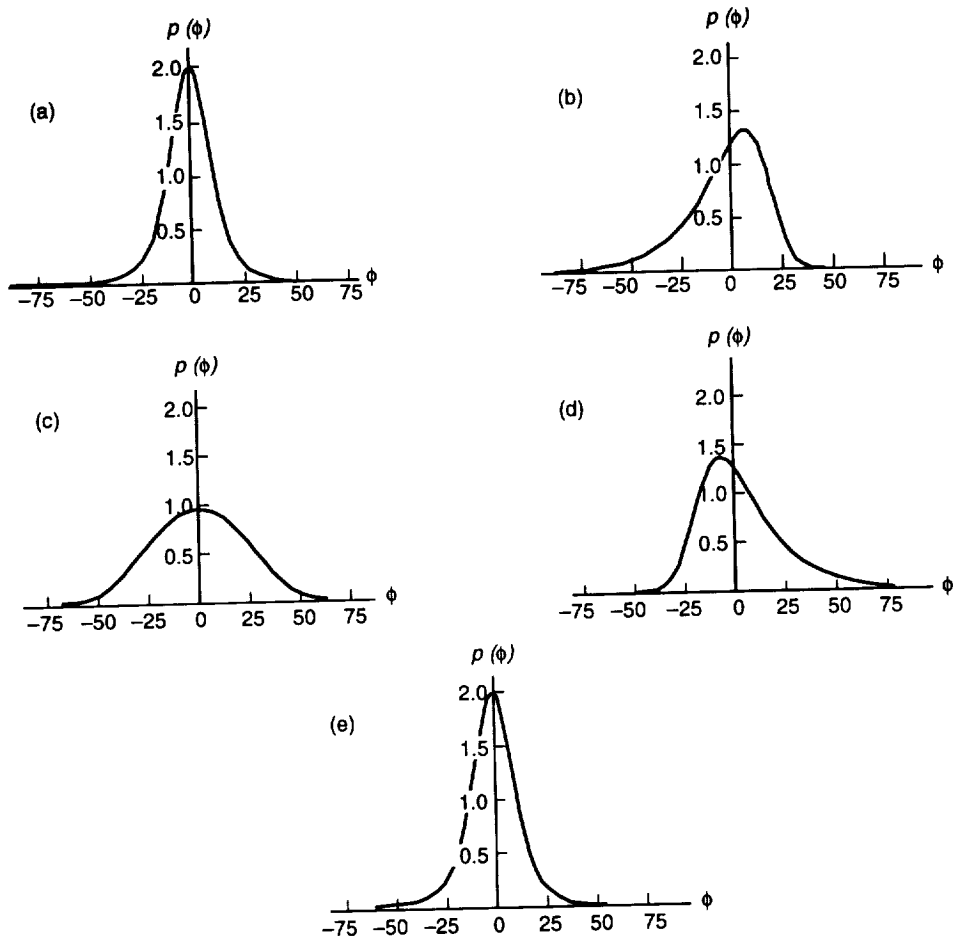

Fig. 9. Phase estimate densities: (a) $\rho = 0.8$, $\psi = 0$ deg, (b) $\rho = 0.8$, $\psi = 45$ deg, (c) $\rho = 0.8$, $\psi = 90$ deg, (d) $\rho = 0.8$, $\psi = 135$ deg, and (e) $\rho = 0.8$, $\psi = 180$ deg.

$$SNR' = \frac{2P_{T1}}{N_{o1}R_{sym}} \frac{\sum_{i=1}^{L}\gamma_i^2 + \sum_{i=1}^{L}\sum_{\substack{j=1\\i\neq j}}^{L}\gamma_i\gamma_j e^{j(\Delta\phi_{1i}-\Delta\phi_{1j})}}{\sum_{i=1}^{L}\gamma_i + \sum_{i=1}^{L}\sum_{\substack{j=1\\i\neq j}}^{L}(\gamma_i\gamma_j)^{1/2}\rho_{ij}e^{j\psi_{ij}}\ e^{j(\Delta\phi_{1i}-\Delta\phi_{1j})}} C_c^2 C_{sc}^2 C_{sy}^2 \tag{41}$$

where C_c, C_{sc}, and C_{sy} are the carrier, subcarrier, and symbol reduction functions, respectively. The unconditional symbol SNR is obtained by integrating Eq. (41) over the density functions for $\hat{\phi}_{21}, \cdots, \hat{\phi}_{L1}$ and the loop errors ϕ_c, ϕ_{sc}, and ϕ_{sy}. In order to simplify this computation, the loop errors and phase estimates are generally assumed to be independent. Taking expectation with respect to each of these quantities separately yields an expression for the unconditional symbol SNR, namely

$$\begin{aligned} SNR = {} & \frac{2P_{T1}}{N_{o1}R_{sym}} \overline{C_c^2}\ \overline{C_{sc}^2}\ \overline{C_{sy}^2} \\ & \times \int_{-\pi}^{\pi}\cdots\int_{-\pi}^{\pi}\left[\frac{\sum_{i=1}^{L}\gamma_i^2 + \sum_{i=1}^{L}\sum_{\substack{j=1\\i\neq j}}^{L}\gamma_i\gamma_j e^{j(\Delta\phi_{1i}-\Delta\phi_{1j})}}{\sum_{i=1}^{L}\gamma_i + \sum_{i=1}^{L}\sum_{\substack{j=1\\i\neq j}}^{L}(\gamma_i\gamma_j)^{1/2}\rho_{ij}\ e^{j\psi_{ij}}\ e^{j(\Delta\phi_{1i}-\Delta\phi_{1j})}} p(\Delta\phi_{1i})\cdots p(\Delta\phi_{1L})\right] \\ & \times d\Delta\phi_{12}\cdots d\Delta\phi_{1L} \end{aligned} \tag{42}$$

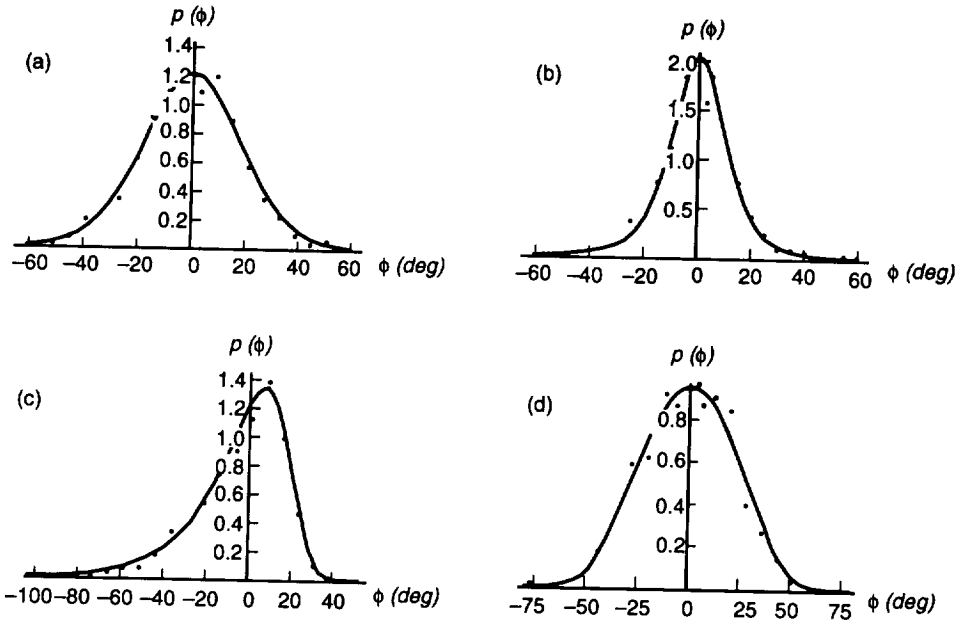

Fig. 10. Phase estimate densities with simulation points: (a) ρ = 0.0, (b) ρ = 0.8, ψ = 0 deg, (c) ρ = 0.8, ψ = 45 deg, and (d) ρ = 0.8, ψ = 90 deg.

where the density functions $p_\phi(\Delta\phi_{1i})$ are as given in Appendix A. Finally, taking the ratio of Eq. (42) to the ideal SNR, Eq. (25), yields the degradation for full-spectrum combining:

$$D_{fsc} = \overline{C_c^2}\,\overline{C_{sc}^2}\,\overline{C_{sy}^2}$$

$$\times \int_{-\pi}^{\pi} \cdots \int_{-\pi}^{\pi} \left[\frac{\sum_{i=1}^{L} \gamma_i^2 + \sum_{i=1}^{L} \sum_{\substack{j=1 \\ i \neq j}}^{L} \gamma_i \gamma_j e^{j(\Delta\phi_{1i} - \Delta\phi_{1j})}}{\sum_{i=1}^{L} \gamma_i + \sum_{i=1}^{L} \sum_{\substack{j=1 \\ i \neq j}}^{L} (\gamma_i \gamma_j)^{1/2} \rho_{ij}\, e^{j\psi_{ij}}\, e^{j(\Delta\phi_{1i} - \Delta\phi_{1j})}} p(\Delta\phi_{1i}) \cdots p(\Delta\phi_{1L}) \right]$$

$$\times\, d\Delta\phi_{12} \cdots d\Delta\phi_{1L}\; G_A^{-1} \tag{43}$$

Note that D_{fsc} is equal to one in the upper limit, where $\Delta\phi_{1i} = 0$ for $i = 2, \cdots, L$ and $\overline{C_c^2} = \overline{C_{sc}^2} = \overline{C_{sy}^2} = 1$. The second moments of the reduction functions $\overline{C_c^2}, \overline{C_{sc}^2}$, and $\overline{C_{sy}^2}$ can be expressed in terms of the loop SNRs of the three loops, and are given in [1].

C. Simulation Results

A simple two-antenna array was simulated under conditions of correlated noise to verify the analysis given above. The symbol SNR of the combined data was measured using the split-symbol moments estimator and divided by the ideal symbol SNR to obtain measured degradations. The signal parameters used were $P_{T_1}/N_{o_1} = P_{T_2}/N_{o_2} = 25$ dB-Hz, $R_{sym} = 200$ symbols per second (sps), and $\Delta = 90$ deg. The carrier, subcarrier, and symbol loops were operated with bandwidths of 3.5, 0.75, and 0.15 Hz, respectively, with a symbol window of 1/2. The correlation coefficient between the noises, ρ, and the relative noise phase, ψ, were varied over a range of values.

Figure 11 shows simulation values along with curves describing analytical results for a "high" correlator SNR. The correlation bandwidths and integration time were chosen so that degradation resulting from

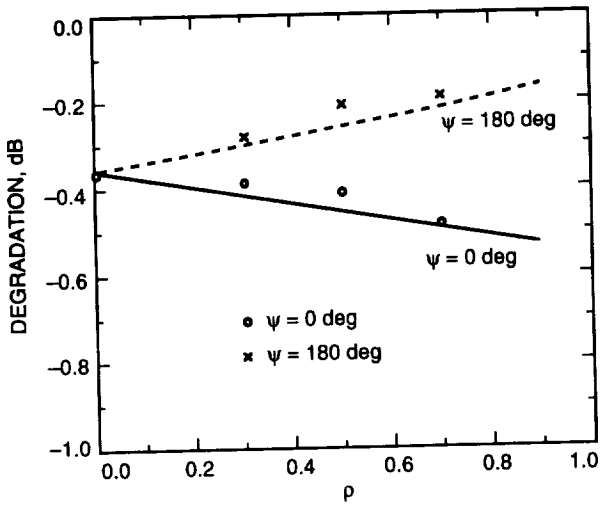

Fig. 11. FSC degradation, high correlator SNR—theory and simulation.

imperfect phasing is negligible compared to the carrier, subcarrier, and symbol losses. The curves show that more degradation is incurred with increasing noise correlation for $\psi = 0$ deg, and that degradation decreases as ρ increases for $\psi = 180$ deg.[4] This can be explained by noting the effect of varying ρ and ψ on the arraying gain. For $\psi = 0$ deg, increasing ρ causes a decrease in arrayed symbol SNR, as explained in Section III.A. The loop SNR of the three loops, therefore, decreases, resulting in more carrier, subcarrier, and symbol loss. By contrast, when $\psi = 180$ deg, increasing ρ increases the combined P_T/N_o and raises the three loop SNRs. This results in *less* degradation in demodulating the signal. Since the correlator SNR is high in this example, the demodulation losses are the dominant source of degradation, and the trend shown in Fig. 11 is thus explained.

Figure 12 shows the same results performed for a relatively "low" correlator SNR. Here, the degradation curve for $\psi = 180$ deg actually lies *below* the curve for $\psi = 0$ deg. This result, although seemingly counter-intuitive, can nevertheless be explained qualitatively. Note from Eq. (41) that the phase error terms $\Delta\phi_{1i}$ appear in both the numerator *and* the denominator of the SNR expression; the phase errors affect both the arrayed signal power and the arrayed noise power. This is in contrast to the uncorrelated noise case, where only the numerator depends on the phase errors $\Delta\phi_{1i}$; since the noises are uncorrelated, the choice of phases used in combining them does not affect their arrayed power. The phase errors $\Delta\phi_{1i}$ always decrease the arrayed signal power, but can decrease *or* increase the arrayed noise power, depending on the phase parameter ψ. For $\psi = 180$ deg, the noise power is increased by errors in estimating ϕ_{1i}, since phasing the array perfectly results in maximum noise cancellation. Therefore, estimating the phase imperfectly results in a twofold penalty: The combined signal power is lessened, and the combined noise power increases. This results in increased degradation due to imperfect phase alignment. On the other hand, when $\psi = 0$ deg, phase misalignment *decreases* the arrayed noise power. Since $\phi_{1i} = \phi_{1i}^n$ in this case, aligning the signals imperfectly also lessens the constructive addition of the noise. The reduced noise power due to phasing errors, therefore, has a mitigating effect on the degradation incurred.

It should be noted that the fact that the $\psi = 180$-deg case has more degradation than the $\psi = 0$-deg case in this example does *not* mean that the overall performance of the array is worse for $\psi = 180$ deg. Recall that degradation is defined as the deviation from the ideal arraying gain, G_A. In the above example,

[4] The phrase "decreasing degradation" is used loosely to mean decreased synchronization losses; in actuality, numerically lower degradation implies *greater* losses incurred.

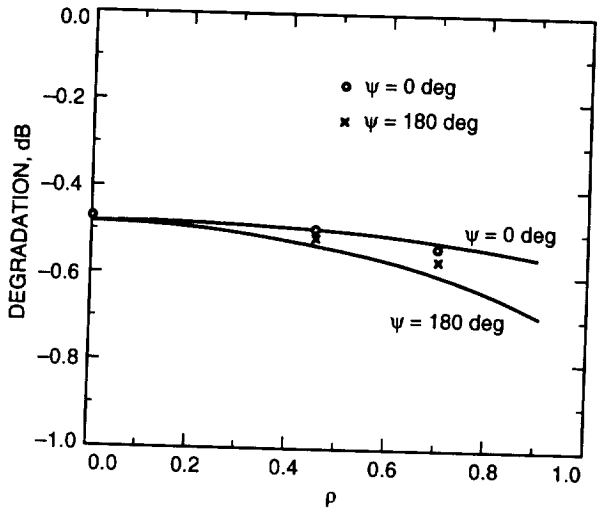

Fig. 12. FSC degradation, low correlator SNR—theory and simulation.

although the degradation for $\psi = 180$ deg is slightly higher, the ideal gain is substantially higher than it is for $\psi = 0$ deg. Thus, to determine the absolute performance for the array in terms of total combined SNR, both the ideal gain and the degradation must be accounted for.

IV. Complex-Symbol Combining Performance

A block diagram of the complex-symbol combining arraying scheme is shown in Fig. 13. Each signal is open-loop downconverted to baseband with quadrature tones and tracked by separate subcarrier and symbol loops. Since the carrier is not tracked coherently, each signal consists of both an "I" and "Q" component, which can be thought of as a single complex signal. Furthermore, since subcarrier and symbol tracking are performed in the absence of carrier lock, the loop SNRs of these loops are different from the case where the carrier is tracked first. Two types of subcarrier and symbol loops that may be used in complex-symbol combining are discussed in [2]: the conventional, or "I" loop, which uses only one of the two signals in the complex pair to track, and the "IQ" loop, which uses both real and imaginary channels. We will assume the IQ loops are used, since they have higher loop SNRs.

The matched filter outputs consist of data modulated by complex baseband tones. These complex symbols are transmitted to a central location for combining. As in the case of full-spectrum combining, correlations are performed to phase align the carriers, after which the signals are weighted and summed coherently. A baseband Costas loop is finally used to demodulate the carrier.

Since the ideal arraying gain G_A is independent of which arraying technique is used, the expression computed in Section III.A is valid for complex-symbol combining also. Thus, it is only necessary to evaluate the degradation for CSC, taking into account combining and demodulation losses. Once again, the presence of correlated noise creates complications in phasing the array. A technique similar to the one used for FSC can be employed to reduce the biases in estimating the relative signal phases, as discussed below.

A. Antenna Phasing

The complex-symbol stream from the ith antenna is given by

$$\tilde{Y}_i(k) = \sqrt{P_{D_i}} C_{sc_i} C_{sy_i}\, d(k)\, e^{j(\omega_b T_s k + \theta_i)} + \tilde{N}_i(k) \tag{44}$$

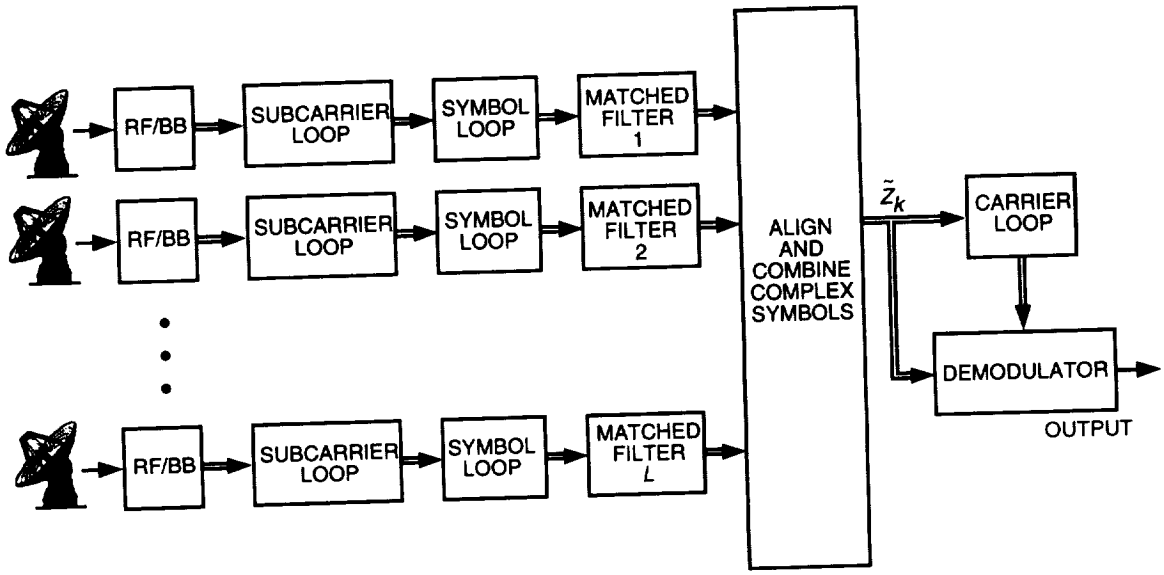

Fig. 13. Complex-symbol combining.

where C_{sc_i} and C_{sy_i} are the subcarrier and symbol reduction functions for the ith receiver, T_s is the symbol time, and $\tilde{N}_i(k)$ is the noise output from the ith matched filter. Taking the complex product between the 1st and ith streams yields

$$Z = \tilde{Y}_1(k)\tilde{Y}_i^*(k) = \sqrt{P_{D_1}P_{D_i}}C_{sc_1}C_{sc_i}C_{sy_1}C_{sy_i} + \tilde{N}_{s,n}(k) + \tilde{N}_1(k)\tilde{N}_i^*(k) \tag{45}$$

where the signal-noise term $\tilde{N}_{s,n}(k)$ has zero mean. Once again, the complex-noise product $\tilde{N}_1(k)\tilde{N}_i^*(k)$ has nonzero mean if the correlation coefficient is nonzero and introduces a bias to the signal correlation vector. Note, however, that the spectrum of the signals at the point of combining, $Y_i(k)$, does not contain empty bands as in the case of full-spectrum combining. Demodulating the subcarrier collapses all the data sidebands to baseband, allowing a much narrower combining bandwidth. Since the shared information rate for CSC is equal to the symbol rate, there is *no excess bandwidth that can be used to measure the correlation of the noise alone.* This problem may be solved by adding an extra matched filter for each receiver to capture noise only. Before investigating this possibility, however, we calculate the expectation of the noise product, $E[\tilde{N}_i(k)\tilde{N}_j^*(k)]$.

Consider the block diagram of Fig. 14, which shows the processing for complex-symbol combining up to the matched filter outputs. The signal $s_i(t)$ is the subcarrier reference from the ith subcarrier loop, given by

$$s_i(t) = \mathrm{sqr}(\omega_{sc}t + \theta_{sc} + \phi_{sci}) \tag{46}$$

where θ_{sc} is the instantaneous subcarrier phase and ϕ_{sc_i} is the instantaneous phase error in the ith loop, for $i = 1, \cdots, L$. The limits of integration for the ith matched filter are given by

$$t_{l_i} = kT_s + \tau_i \tag{47}$$

$$t_{u_i} = (k+1)T_s + \tau_i \tag{48}$$

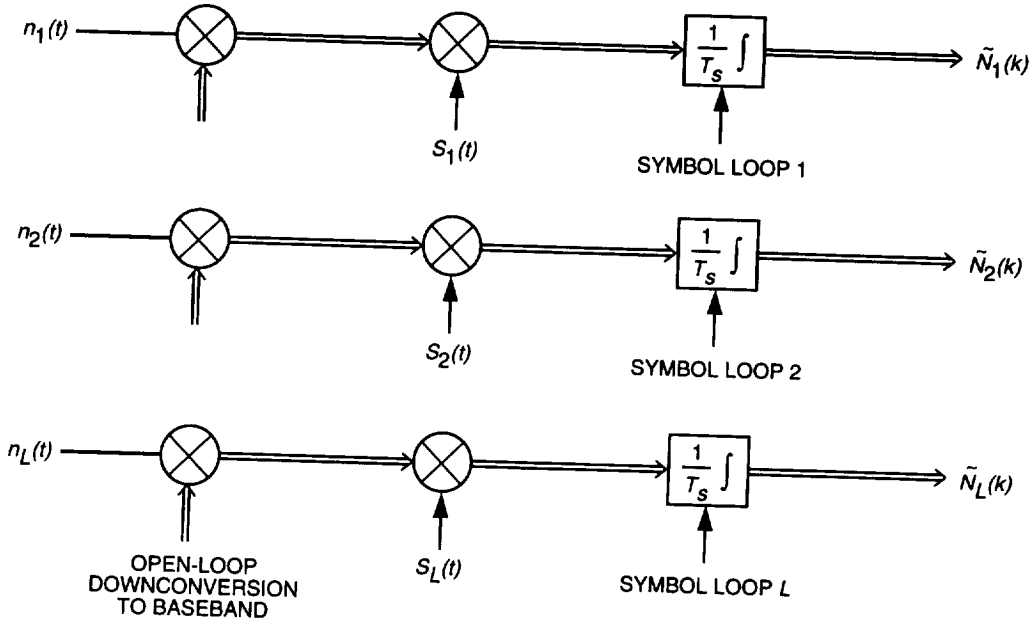

Fig. 14. Matched filter noise outputs for CSC.

where τ_i is the timing error in the ith symbol loop. The matched-filter noise samples are, therefore, given by

$$\tilde{N}_i(k) = \frac{1}{T_s} \int_{kT_s+\tau_i}^{(k+1)T_s+\tau_i} \tilde{n}_i(t)\ \mathrm{sqr}(\omega_{sc}t + \theta_{sc} + \phi_{sc_i})\ dt \tag{49}$$

$$\tilde{N}_j(k) = \frac{1}{T_s} \int_{kT_s+\tau_j}^{(k+1)T_s+\tau_j} \tilde{n}_j(t)\ \mathrm{sqr}(\omega_{sc}t + \theta_{sc} + \phi_{sc_j})\ dt \tag{50}$$

The conditional expectation of $\tilde{N}_i(k)\tilde{N}_j^*(k)$ given the subcarrier and symbol timing errors can then be calculated by combining the above expressions with the cross-correlation function for the complex baseband noises, i.e.,

$$R_{\tilde{n}_i,\tilde{n}_j}(u,v) = E\left[\tilde{n}_i(u)\tilde{n}_j^*(v)\right] = \alpha_{ij}\ e^{j\phi_{ij}^n}\ \delta(u-v) \tag{51}$$

yielding

$$\begin{aligned} E\left[\tilde{N}_i(k)\tilde{N}_j^*(k)\right] &= \frac{1}{T_s^2} E\left[\int_{kT_s+\tau_i}^{(k+1)T_s+\tau_i}\int_{kT_s+\tau_j}^{(k+1)T_s+\tau_j} \tilde{n}_i(u)s_i(u)\ \tilde{n}_j^*(v)s_j(v)\ du\ dv\right] \\ &= \frac{\alpha_{ij}e^{j\phi_{ij}^n}}{T_s^2} \int_{kT_s+\tau_i}^{(k+1)T_s+\tau_i}\int_{kT_s+\tau_j}^{(k+1)T_s+\tau_j} \delta(u-v)\ s_i(u)s_j(v)\ du\ dv \\ &= \frac{\alpha_{ij}e^{j\phi_{ij}^n}}{T_s^2} \int_{t_{min}}^{t_{max}} s_i(v)s_j(v)\ dv \end{aligned} \tag{52}$$

where the limits of integration of v are given by

$$t_{min} = \max(kT_s + \tau_i,\ kT_s + \tau_j) \tag{53}$$

$$t_{max} = \min\left((k+1)T_s + \tau_i,\ (k+1)T_s + \tau_j\right) \tag{54}$$

Finally, integrating with respect to v yields

$$E\left[\tilde{N}_i(k)\tilde{N}_j^*(k)\right] = \frac{\alpha_{ij}e^{j\phi_{ij}^n}}{T_s^2}\left(1 - \frac{2}{\pi}|\phi_{sc_i} - \phi_{sc_j}|\right)\left(T_s - |\tau_i - \tau_j|\right) \tag{55}$$

$$= \frac{\alpha_{ij}e^{j\phi_{ij}^n}}{T_s}\left(1 - \frac{2}{\pi}|\phi_{sc_i} - \phi_{sc_j}|\right)\left(1 - \frac{1}{2\pi}|\phi_{sy_i} - \phi_{sy_j}|\right) \tag{56}$$

$$= \alpha_{ij}e^{j\phi_{ij}^n}\ R_{sym}\ C_{sc_{ij}}\ C_{sy_{ij}} \tag{57}$$

Note that, in the absence of phase errors in any of the loops, Eq. (57) reduces to $\alpha_{ij}e^{j\phi_{ij}^n}R_{sym}$, which is simply the cross-power spectral density of the noises $\tilde{n}_i(t)$ and $\tilde{n}_j(t)$ times the effective bandwidth of the matched filter. Thus, in addition to reducing the effective signal power at the matched filter output, the subcarrier and symbol phase errors *also* reduce the noise correlation at this point.

Calculating the unconditional covariance of the matched filter noises requires taking the expectation of Eq. (57) with respect to the phase errors $\phi_{sc_i}, \phi_{sc_j}, \phi_{sy_i}$, and ϕ_{sy_j}. Two approximations are made to perform this computation. First, the densities of the phase errors are assumed to be Gaussian. This condition is nearly satisfied for loop SNRs above 10 dB and is consistent with the approximation made in [1]. Second, the phase errors of all loops are assumed to be mutually independent. This statement is not strictly justifiable, since the subcarrier and symbol loops from a single receiver are affected by the same noise and, furthermore, because the noises viewed by separate receivers are correlated. Nevertheless, it is invoked for the purpose of making a first-order approximation to evaluating the unconditional covariance. The quantities $\phi_{sc_i} - \phi_{sc_j}$ and $\phi_{sy_i} - \phi_{sy_j}$ are then Gaussian-distributed with known mean and variance, and the unconditional expectation $E[\tilde{N}_i(k)\tilde{N}_j^*(k)]$ becomes

$$E\left[\tilde{N}_i(k)\tilde{N}_j^*(k)\right] = \alpha_{ij}e^{j\phi_{ij}^n}R_{sym}\overline{C_{sc_{ij}}}\ \overline{C_{sy_{ij}}} = \rho_{ij}\sqrt{N_{o_i}N_{o_j}}e^{j\phi_{ij}^n}\ R_{sym}\left(1 - \frac{2}{\pi}\sqrt{\frac{2}{\pi}}(\sigma^2_{\phi_{sc_i}} + \sigma^2_{\phi_{sc_j}})^{1/2}\right)$$

$$\times\left(1 - \frac{1}{2\pi}\sqrt{\frac{2}{\pi}}\left(\sigma^2_{\phi_{sy_i}} + \sigma^2_{\phi_{sy_j}}\right)^{1/2}\right) \tag{58}$$

Equations (58) and (45) can be combined to calculate the ratio of the signal-to-noise correlation magnitude, analogous to that computed in (29):

$$\frac{|\vec{S}|}{|\vec{N}|} = \frac{\sqrt{P_{D_1}P_{D_i}}\ \overline{C_{sc_1}}\ \overline{C_{sy_1}}\ \overline{C_{sc_i}}\ \overline{C_{sy_i}}}{\rho_{ij}\sqrt{N_{o_1}N_{o_i}}R_{sym}\ \overline{C_{sc_{ij}}}\ \overline{C_{sy_{ij}}}} \approx \frac{1}{\rho_{ij}}\left(\frac{E_{s_1}}{N_{o_1}}\frac{E_{s_i}}{N_{o_i}}\right)^{1/2} \tag{59}$$

where $E_s/N_o = P_D T_s/N_o$ is the bit SNR. In making the approximation of Eq. (59), the effects of synchronization have been ignored for simplicity. This result provides a useful rule of thumb for determining if the

noise correlation is a significant bias in estimating the relative signal phase. If $|\vec{S}|/|\vec{N}|$ is much less than 1, then an extra correlation is needed to compensate for the noise vector, as mentioned earlier. On the other hand, if this quantity is much greater than 1, then it is unnecessary to add the extra matched filter channel to perform the noise-only correlation. Note that collapsing all the data sidebands to baseband and performing matched filtering *before* the correlation takes place substantially decreases the correlation bandwidth relative to that of the FSC scheme described in [2]. The full-spectrum combining scheme can optionally be modified to employ a similar strategy by using a series of matched filters for each subcarrier harmonic, as discussed earlier. Estimating the degree of correlation ρ that will be observed for a particular antenna pair and applying the rule described above will indicate whether or not the noise contribution to the total correlation is substantial and must be compensated for by performing an additional correlation.

Here we briefly describe how the extra matched-filter outputs can be used to measure the noise correlation: The complex baseband signal from each antenna can be shifted in frequency so that an empty portion of the spectrum is located at baseband. This may be accomplished by shifting by an even multiple of the subcarrier frequency, i.e.,

$$\tilde{y}_i'(t) = \left(\sqrt{P_{C_i}}e^{j(\omega_b t+\theta_i)} + j\sqrt{P_{D_i}}d(t)\ \mathrm{sqr}(\omega_{sc}t+\theta_{sc})e^{j(\omega_b t+\theta_i)} + \tilde{n}_i(t)\right)e^{jN\omega_{sc}t} = \tilde{s}_i'(t) + \tilde{n}_i'(t) \qquad (60)$$

where N is an even integer. The shifted signal can then be multiplied by the subcarrier reference from the ith antenna and passed through a matched filter using timing from the ith symbol loop, as shown in Fig. 14. Thus,

$$\tilde{N}_i'(t) = \frac{1}{T_s}\int_{kT_s+\tau_i}^{(k+1)T_s+\tau_i} \tilde{n}_i'(t)\ \mathrm{sqr}(\omega_{sc}t+\theta_{sc}+\phi_{sc_i})\ dt \qquad (61)$$

From the above analysis, it is clear that $E[\tilde{N}_i'(k)\tilde{N}_j'(k)]$ will be given by Eq. (58). Correlating the two noise-only matched filter outputs then yields a quantity that can be subtracted from the total correlation, Z, to compensate for the noise bias. The density function for the phase estimate computed using this technique is similar to the FSC case and is analyzed in Appendix B. Note, however, that performing this compensation requires increasing the combining bandwidth beyond what is required for CSC in the uncorrelated noise case, as well as additional hardware to process the extra channel containing noise only. A tradeoff in performance versus complexity must, therefore, be made to determine if complex-symbol combining is an attractive option when correlated noise is present.

B. Arrayed Symbol SNR and Symbol SNR Degradation

An expression for the conditional arrayed symbol SNR can be obtained in a similar manner as is the full-spectrum combining case. The combined signal for complex-symbol combining is given by

$$\tilde{Y}_{comb}(k) = \tilde{S}_{comb}(k) + \tilde{N}_{comb}(k) = \sum_{i=1}^{L}\beta_i e^{j\hat{\phi}_{1i}}\left(\sqrt{P_{D_i}}C_{sc_i}C_{sy_i}d(k)e^{j(\omega_b T_s k+\theta_i)} + \tilde{N}_i(k)\right) \qquad (62)$$

The conditional signal power, defined as $E[\tilde{S}_{comb}(k)]E[\tilde{S}_{comb}^*(k)]$, is given by

$$P_{comb} = P_{D_1}\left(\sum_{i=1}^{L}\gamma_i^2 C_{sc_i}^2 C_{sy_i}^2 + \sum_{i=1}^{L}\sum_{\substack{j=1\\ i\neq j}}^{L}\gamma_i\gamma_j C_{sc_i}C_{sc_j}C_{sy_i}C_{sy_j}\ e^{j(\Delta\phi_{1i}-\Delta\phi_{1j})}\right) \qquad (63)$$

where, as before, $\Delta\phi_{1i}$ is defined as the error in estimating the phase difference between the 1st and ith signal, $\hat{\phi}_{1i} - \phi_{1i}$. The one-sided power spectral density of the real and imaginary parts of $\tilde{N}_{comb}(k)$ is given by

$$N_o = T_s \; Var \; \left(\tilde{N}_{comb}(k)\right) = T_s \; E\left[\left(\sum_{i=1}^{L} \beta_i e^{j\hat{\phi}_{1i}} \tilde{N}_i(k)\right) \times \left(\sum_{j=1}^{L} \beta_j e^{-j\hat{\phi}_{1j}} \tilde{N}_j^*(k)\right)\right] \tag{64}$$

Using the relations

$$E[\tilde{N}_i(k)\tilde{N}_i^*(k)] \; = \frac{N_{o_i}}{T_s} \tag{65}$$

$$E[\tilde{N}_i(k)\tilde{N}_j^*(k)] \; = \frac{\rho_{ij}\sqrt{N_{o_i}N_{o_j}}\; e^{\phi_{ij}^n}}{T_s}\; \overline{C_{sc_{ij}}}\; \overline{C_{sy_{ij}}} \tag{66}$$

Eq. (64) can be shown to be equal to

$$N_o' = N_{o_1}\left(\sum_{i=1}^{L}\gamma_i + \sum_{i=1}^{L}\sum_{\substack{j=1\\ i\neq j}}^{L}\sqrt{\gamma_i\gamma_j}\rho_{ij}C_{sc_{ij}}C_{sy_{ij}}e^{j\psi_{ij}}e^{j\left(\Delta\phi_{1i}^n - \Delta\phi_{1j}^n\right)}\right) \tag{67}$$

Taking the ratio of Eq. (63) to Eq. (67) then yields the combined P_D/N_o for CSC. The combined signal is finally processed by a baseband Costas loop, and the conditional SNR adding in carrier losses is given by

$$SNR' = \frac{2P_{D_1}}{N_{o_1}R_{sym}}\; \frac{\sum_{i=1}^{L}\gamma_i^2 C_{sc_i}^2 C_{sy_i}^2 + \sum_{i=1}^{L}\sum_{\substack{j=1\\ i\neq j}}^{L}\gamma_i\gamma_j C_{sc_i}C_{sc_j}C_{sy_i}C_{sy_j}e^{j(\Delta\phi_{1i}-\Delta\phi_{1j})}}{\sum_{i=1}^{L}\gamma_i + \sum_{i=1}^{L}\sum_{\substack{j=1\\ i\neq j}}^{L}\sqrt{\gamma_i\gamma_j}\rho_{ij}C_{sc_{ij}}C_{sy_{ij}}e^{j\psi_{ij}}e^{j(\Delta\phi_{1i}-\Delta\phi_{1j})}}\; C_c^2 \tag{68}$$

Computing the unconditional symbol SNR requires taking the expectation of the above quantity with respect to the phase errors ϕ_{sc_i} and ϕ_{sy_i} for $i = 1, \cdots, L$, the phase estimates $\hat{\phi}_{1i}$ for $i = 2, \cdots, L$, and the carrier phase error ϕ_c. Once again, we assume all loop phase errors and phase-aligning errors are mutually independent. Thus, integration over the carrier phase error ϕ_c is accomplished easily by considering the carrier reduction function C_c^2 separately. However, unlike the case of full-spectrum combining, the subcarrier and symbol phase errors appear in both the numerator *and* the denominator. The expectation with respect to the subcarrier and symbol phase errors, therefore, cannot be given in closed form. Calculating the unconditional symbol SNR for even a simple two-element array would thus require a fifth-order numerical integration. Rather than resort to such brute-force tactics, we make further simplifying assumptions to allow evaluation of some of the integrals in closed form.

In taking the expectation with respect to the ϕ_{sc_i} and ϕ_{sy_i} terms, we apply the approximation

$$E\left[\frac{x}{y}\right] \approx \frac{E[x]}{E[y]} \tag{69}$$

to the ratio of Eq. (68), yielding

$$SNR = \frac{2P_{d1}}{N_{o1}R_{sym}}$$

$$\times E_{\hat{\Phi}}\left[\frac{E_{\Phi_{sc},\Phi_{sy}|\hat{\Phi}}\left[\sum_{i=1}^{L}\gamma_i^2 C_{sc_i}^2 C_{sy_i}^2 + \sum_{i=1}^{L}\sum_{\substack{j=1\\ i\neq j}}^{L}\gamma_i\gamma_j C_{sc_i}C_{sc_j}C_{sy_i}C_{sy_j}e^{j(\Delta\phi_{i1}-\Delta\phi_{j1})}\right]}{E_{\Phi_{sc},\Phi_{sy}|\hat{\Phi}}\left[\sum_{i=1}^{L}\gamma_i + \sum_{i=1}^{L}\sum_{\substack{j=1\\ i\neq j}}^{L}\sqrt{\gamma_i\gamma_j}\rho_{ij}C_{sc_{ij}}C_{sy_{ij}}e^{j\psi_{ij}}e^{j(\Delta\phi_{1i}-\Delta\phi_{1j})}\right]}\right]\overline{C_c^2} \quad (70)$$

where Φ_{sc} is the set of subcarrier phase errors ϕ_{sc_i} for $i = 1, \cdots, L$, Φ_{sy} is the set of symbol phase errors ϕ_{sy_i} for $i = 1, \cdots, L$, and $\hat{\Phi}$ is the set of phase estimates $\hat{\phi}_{1i}$ for $i = 2, \cdots, L$. The approximation of Eq. (69) is reasonable if the mean of y squared is much greater than the variance of y (i.e., if y is nearly a constant). This condition is met for the case under consideration, since it is implicitly assumed that the loop SNRs of the subcarrier and symbol loops are high enough to maintain lock, with 13 dB being a typical threshold. Thus, the variances of the reduction functions $C_{sc_{ij}}$ and $C_{sy_{ij}}$, which contain the loop phase errors, will be small compared to the mean of the entire denominator term.

By the above argument, the unconditional SNR can be evaluated as

$$SNR = \frac{2P_{D_1}}{N_{o_1}R_{sym}}\overline{C_c^2}$$

$$\times \int_{-\pi}^{\pi}\cdots\int_{-\pi}^{\pi}\left[\frac{\sum_{i=1}^{L}\gamma_i^2\overline{C_{sc_i}^2}\;\overline{C_{sy_i}^2} + \sum_{i=1}^{L}\sum_{\substack{j=1\\ i\neq j}}^{L}\gamma_i\gamma_j\overline{C_{sc_i}}\;\overline{C_{sc_j}}\;\overline{C_{sy_i}}\;\overline{C_{sy_j}}e^{j(\Delta\phi_{1i}-\Delta\phi_{1j})}}{\sum_{i=1}^{L}\gamma_i + \sum_{i=1}^{L}\sum_{\substack{j=1\\ i\neq j}}^{L}\sqrt{\gamma_i\gamma_j}\rho_{ij}\overline{C_{sc_{ij}}}\;\overline{C_{sy_{ij}}}e^{j\psi_{ij}}e^{j(\Delta\phi_{1i}-\Delta\phi_{1j})}}\right.$$

$$\left.\times\, p(\Delta\phi_{12})\cdots p(\Delta\phi_{1L})\right]d\Delta\phi_{12}\cdots d\Delta\phi_{1L} \quad (71)$$

The ideal symbol SNR for complex-symbol combining is identical to that for full-spectrum combining; since SNR_{ideal} is defined as the SNR that would be obtained in the absence of synchronization errors, its value is independent of the order in which combining and demodulation occur. Thus, the degradation for complex-symbol combining is found by combining the results of Eq. (71) with Eq. (25), yielding

$$D_{csc} = \overline{C_c^2}$$

$$\times \int_{-\pi}^{\pi}\cdots\int_{-\pi}^{\pi}\left[\frac{\sum_{i=1}^{L}\gamma_i^2\overline{C_{sc_i}^2}\;\overline{C_{sy_i}^2} + \sum_{i=1}^{L}\sum_{\substack{j=1\\ i\neq j}}^{L}\gamma_i\gamma_j\overline{C_{sc_i}}\;\overline{C_{sc_j}}\;\overline{C_{sy_i}}\;\overline{C_{sy_j}}e^{j(\Delta\phi_{i1}-\Delta\phi_{j1})}}{\sum_{i=1}^{L}\gamma_i + \sum_{i=1}^{L}\sum_{\substack{j=1\\ i\neq j}}^{L}\sqrt{\gamma_i\gamma_j}\rho_{ij}\overline{C_{sc_{ij}}}\;\overline{C_{sy_{ij}}}e^{j\psi_{ij}}e^{j(\Delta\phi_{i1}^n-\Delta\phi_{j1}^n)}}\right.$$

$$\left.\times\, p(\Delta\phi_{12})\cdots p(\Delta\phi_{1L})\right]d\Delta\phi_{12}\cdots d\Delta\phi_{1L}\; G_A^{-1} \quad (72)$$

C. Simulation Results

Simulations of a two-antenna complex-symbol combining system were performed. The signal parameters used were the same as those used for the full-spectrum combining simulations: $P_{T_1}/N_{o_1} = P_{T_2}/N_{o_2} = 25$ dB-Hz, $R_{sym} = 200$ sps, and $\Delta = 90$ deg. The loop bandwidths were also set as before; the

carrier, subcarrier, and symbol loop bandwidths were 3.5, 0.75, and 0.15 Hz, respectively, with a symbol window of 1/2. Both the compensating and noncompensating methods of estimating the signal phase difference were implemented. In Figs. 15 and 16, simulated and analytical degradation values are shown for various values of ρ and ψ.

For the uncompensated case, the degradation curve drops down sharply for $\psi = 90$ deg and $\psi = 180$ deg. One cause for this is the bias in the complex correlation used to estimate the relative signal phase. For the parameters being used, $|\vec{S}|/|\vec{N}|$, given by Eq. (59), is equal to 3.15 for $\rho = 0.5$. Thus, the noise vector is of comparable but lesser magnitude to that of the signal in estimating the phase. Note that for $\psi = 0$ deg, the noise correlation phase is equal to the relative signal phase ($\phi = \phi^n$), and the vectors $\vec{S}$ and $\vec{N}$ are colinear (see Fig. 5). The noise vector, therefore, does not bias the measurement away from the desired quantity, and the downward trend is not present.

For the compensated case, less overall degradation is observed. However, the $\psi = 180$-deg curve still drops down with increasing ρ. Recall from Section IV.A that imperfect subcarrier and symbol tracking tend to decrease the power levels of the individual signals at the matched filter output *and* decrease the correlation of the matched filter noises. When $\psi = 0$ deg, this has a beneficial effect on the arrayed SNR, since it reduces the coherent addition of the noise. By contrast, when $\psi = 180$ deg, a high degree of correlation between the noises is desirable, so that the noise cancels maximally. Thus, decreasing this correlation lessens the arrayed SNR and causes more degradation. This explains the fact that the $\psi = 0$-deg curve tends upwards with increasing ρ, while the $\psi = 180$-deg tends downward. Note, however, that the reverse trend is true of the ideal arraying gain, G_A. For example, for $\rho = 0.8$, $G_A = 10$ dB for $\psi = 180$ deg, but only 0.46 dB for $\psi = 0$ deg.

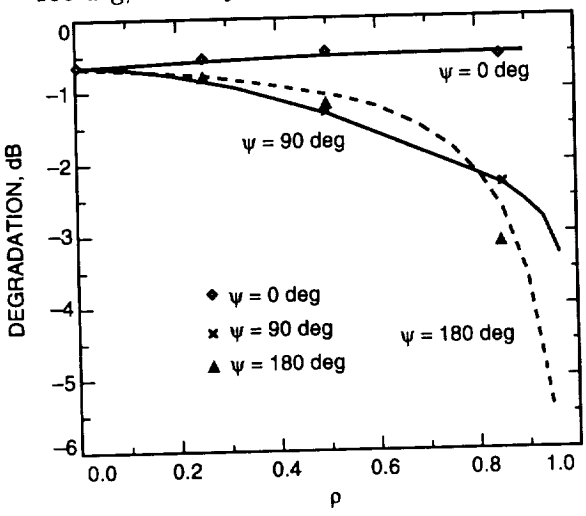

Fig. 15. CSC degradation, phase uncompensated: theory and simulation.

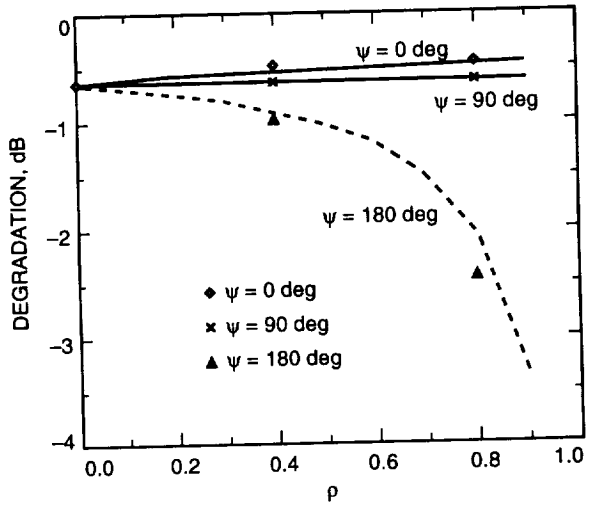

Fig. 16. CSC degradation, phase compensated: theory and simulation.

V. Example: Galileo Scenario

In order to illustrate the major concepts presented in this article, the performance of full-spectrum combining and complex-symbol combining is analyzed for the Galileo signal. An array of DSS 14, which is a 70-m antenna, and DSS 15, a 34-m high-efficiency (HEF) antenna, is chosen for this example. First, predicts for physical parameters describing the signal strength and degree of noise correlation are developed. These quantities are then used to calculate the arraying gain and degradation for each of the two schemes.

A. Signal Parameters

In the case of the Galileo spacecraft, correlated noise will be contributed by Jupiter being in the beam of both antennas. As discussed in Section II, the contribution of a background body to total system noise depends on its angular separation from the spacecraft and on its total flux, which varies with its distance from Earth. Values for the Jupiter–Earth probe (JEP) angle and Jupiter–Earth distance can be found from ephemeris information for the Galileo tour. For the purpose of this example, we select values that maximize the noise contribution of the planet to estimate the impact of correlated noise in a worst-case scenario. Thus, we assume the JEP angle is zero and that the Jupiter–Earth range is at its minimum value during the tour, which is $R_j = 4.0$ AU. Using these values, the temperature contribution of Jupiter for DSS 14 and DSS 15 are $T_{s_1} = 6.6$ K and $T_{s_2} = 1.4$ K, respectively. Note that the temperature contribution is higher for DSS 14 due to the greater aperture size and antenna efficiency.

The predicted signal parameters are as follows: $(P_T/N_o)_1 = 22.0$ dB-Hz and $(P_T/N_o)_2 = 11.6$ dB-Hz for the 70- and 34-m antennas, respectively; $\Delta = 90$ deg; and $R_{sym} = 200$ sps. Note that since we are assuming that the planet and spacecraft are at their closest range, the spacecraft signal is *also* at its peak strength, in addition to the noise contribution of Jupiter. The total system temperatures predicted for DSS 14 and DSS 15 are 22.6 and 42.2 K, respectively.[5]

To determine the degree to which the source is resolved on this array baseline, we must compare the fringe spacing to the angular size of the source. In our example, the observing frequency f_o is 2.3×10^9 Hz, and the maximum possible projected baseline is the physical separation between the two antennas, which is approximately 500 m. Thus, the smallest possible fringe spacing is 2.5×10^{-4} rad. At a range of 4.0 AU, Jupiter has an angular size on the order of 1×10^{-3} rad. Since these values are comparable, we cannot use either the long baseline limit or the short baseline limit in evaluating ρ (see Section I). However, for the purpose of determining the impact of the correlated noise in the most extreme case, we overestimate the degree of noise correlation using the upper bound on ρ, given by

$$\rho = \sqrt{\frac{T_{s_1} T_{s_2}}{T_1 T_2}} \approx 0.1 \tag{73}$$

B. Arraying Performance

Using the two P_T/N_o levels and correlation coefficient ρ found above, the ideal arraying gain G_A can be computed as a function of ψ using Eq. (25). A graph showing this relationship is shown in Fig. 17. Note that the arraying gain in this example is much smaller compared to our previous examples of two equal antennas, since the signal level of one antenna is approximately 10 dB lower than the other. For $\psi = 0$ deg, the correlated component of the noise adds maximally in phase, thus decreasing the arraying gain. By contrast, the background noise interferes destructively for $\psi = 180$ deg, resulting in greater arraying gain. Since the correlation coefficient is relatively low in this example, the difference between the best-case and worst-case scenarios is only about 0.45 dB.

Representative values for the carrier, subcarrier, and symbol loop bandwidths were chosen as 1.5, 0.4, and 0.07 Hz, respectively. For full-spectrum combining, a correlation bandwidth of $B_{corr} = 2$ kHz was used, with a correlation time of 15 s. The total degradation for FSC as a function of ψ is shown in Fig. 18, along with simulation points. Because the correlation coefficient ρ is relatively low in this example, the degradation is almost constant with respect to the phase parameter ψ. The combined P_T/N_o only varies by roughly 0.4 dB as ψ ranges from 0 to 180 deg; thus, the loop SNRs of the three loops also do not change much, and synchronization losses remain essentially constant.

[5] Predicts for noise and signal parameters were obtained from the Galileo S-Band Analysis Program (GSAP).

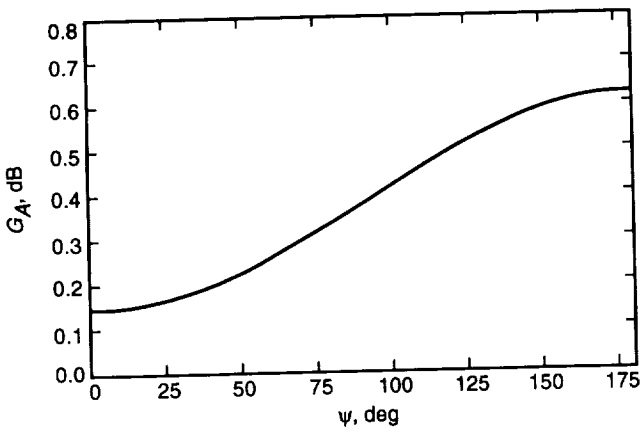

Fig. 17. Ideal arraying gain for Galileo signal parameters.

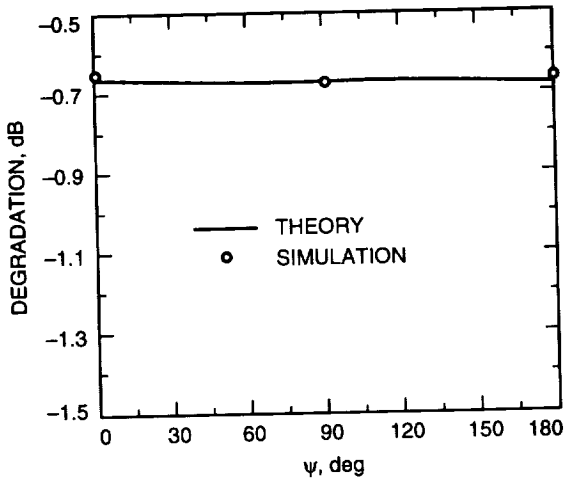

Fig. 18. FSC degradation for Galileo signal parameters.

The same signal parameters and loop bandwidths were used to simulate the complex-symbol combining case. A slight variation of the basic scheme, known as complex-symbol combining with aiding (CSCA), was implemented. This scheme is discussed in [2] as an option for arraying the Galileo signal. In CSCA, the subcarrier and symbol references from the receiver tracking the stronger signal are used to track the signal from the 34-m antenna as well. This technique can be used to perform complex-symbol combining even if the 34-m antenna signal is too weak to achieve subcarrier and symbol lock on its own. Thus, the loop SNRs for the 34-m antenna subcarrier and symbol loops are equal to the corresponding 70-m antenna loop SNRs.

Equation (59) can be applied to determine whether or not the "noise-only" channel is needed to phase the array. Substituting in values from above, we find

$$\frac{1}{\rho}\left(\frac{E_{s_1}}{N_{o_1}}\,\frac{E_{s_2}}{N_{o_2}}\right)^{1/2} = \frac{1}{\rho}\,\frac{1}{R_{sym}}\left(\frac{P_{T_1}}{N_{o_1}}\,\frac{P_{T_2}}{N_{o_2}}\right)^{1/2} \tag{74}$$

$$= 2.39 \tag{75}$$

Thus, the magnitude of the noise correlation vector is less than but comparable to that of the signal correlation vector. To illustrate the impact of the phase bias in aligning the signals, CSCA was simulated with both the compensating and uncompensating method for estimating the relative signal phase. In Fig. 19, we show the degradation for CSCA for these two cases. The correlation time used to estimate the relative signal phase was 2 s. Note that a shorter estimation interval than the full-spectrum combining case can be used here since the effective correlation bandwidth is equal to the data bandwidth of 200 Hz as opposed to 2 kHz for FSC. For the compensated case, the degradation is essentially constant since, once again, the noise correlation does not affect synchronization losses much. For the uncompensated case, the degradation becomes greater as the difference between the noise and signal phase ψ grows larger, since the noise correlation begins to bias the phase estimate further away from the relative signal phase. This effect can be seen graphically by referring once again to Fig. 5, where the complex-signal and noise correlations are represented as vectors.

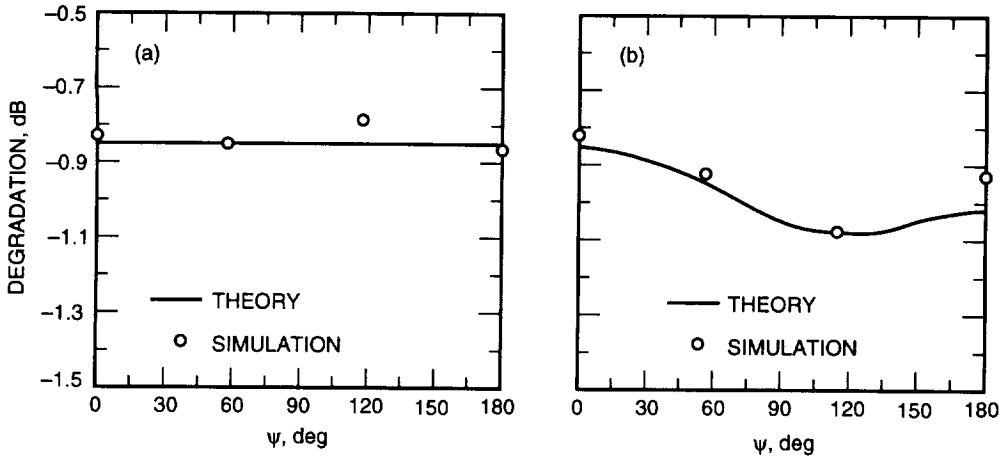

Fig. 19. CSC degradation for Galileo signal parameters: (a) phase compensated and (b) phase uncompensated.

VI. Conclusion

The effects of correlated noise on the full-spectrum combining and complex-symbol combining arraying schemes have been analyzed. As seen in Section II, accurate modeling of the noise correlation properties for a given antenna pair requires detailed analysis of factors such as the source structure and position, the antenna gain patterns, and the geometry of the array. However, the correlation coefficient can be determined easily in cases where the baseline is either very short or very long. These two extreme cases can be used to obtain a rough idea of what degree of noise correlation can be expected for a given scenario.

Describing the correlation between the various antenna pairs in an array by the parameters ρ_{ij} and ψ_{ij}, expressions for the ideal arraying gain and arraying degradation were derived. Several important differences from the uncorrelated noise case were noted. For a given set of signal levels (P_{T_i}/N_{o_i}), the ideal arraying gain when the noise is correlated may be higher *or* lower than when the noise waveforms are independent. This reflects the fact that the noise may add constructively or destructively, depending on the relative signal and noise phases (i.e., the ψ_{ij} parameters).

In addition, correlated noise can have a significant impact on the synchronization processes used to combine and demodulate the signals, which vary with the specific arraying technique used. Most notably, a bias due to the noise correlation is present in the conventional method of estimating the relative signal phases. Since the magnitude of this bias is proportional to the correlation bandwidth used, full-spectrum combining is potentially more sensitive to this problem than complex-symbol combining, depending on the specific method used to correlate the signals. A modified method of phase estimation, where the correlation due to the noise alone is measured and compensated for, can optionally be employed for both FSC and CSC, as necessary.

Acknowledgments

The contributions of numerous individuals to the work described in this article are gratefully acknowledged. I would like to thank David Rogstad and David Meier for their informative discussions on radio interferometry, Sami Hinedi for his insights on arraying techniques, Samson Million for his comments on software simulation methods, and Biren Shah and Mazen Shihabi for their assistance in editing and organizing the article.

References

[1] A. Mileant and S. Hinedi, "Overview of Arraying Techniques for Deep Space Communications," *IEEE Transactions on Communications*, vol. 42, nos. 2/3/4, pp. 1856–1865, February/March/April 1994.

[2] S. Million, B. Shah, and S. Hinedi, "A Comparison of Full-Spectrum and Complex-Symbol Combining Techniques for the Galileo S-Band Mission," *The Telecommunications and Data Acquisition Progress Report 42-116, October–December 1993*, Jet Propulsion Laboratory, Pasadena, California, pp. 128–162, February 15, 1994.

[3] R. Dewey, "The Effects of Correlated Noise in Intra-Complex DSN Arrays for S-Band Galileo Telemetry Reception," *The Telecommunications and Data Acquisition Progress Report 42-111, July–September 1992*, Jet Propulsion Laboratory, Pasadena, California, pp. 129–152, November 15, 1992.

[4] A. Thompson, J. Moran, and G. Swenson, *Interferometry and Synthesis in Radio Astronomy*, New York: John Wiley & Sons, 1986.

[5] H. Tan, "Performance of Residual Carrier Array-Feed Combining in Correlated Noise," *The Telecommunications and Data Acquisition Progress Report 42-121, January–March 1995*, Jet Propulsion Laboratory, Pasadena, California, pp. 131–147, May 15, 1995.

Appendix A

Performance of the FSC Correlator

For full-spectrum combining, the phase difference between two signals is estimated by performing one lowpass and one bandpass correlation, as described in Section III.B. After being filtered to some lowpass bandwidth, B_{lp} Hz, the signals from antenna 1 and antenna i are given by

$$\tilde{y}_{lp_1}(t) = \left[\sqrt{P_{C_1}} + j\sqrt{P_{D_1}}d(t)\left(\frac{4}{\pi}\right)\sum_{\substack{k=1\\ k\ odd}}^{M}\frac{\sin k\omega_{sc}t}{k}\right]e^{(j\omega t+\theta_1)} + \tilde{n}_{lp_1}(t) \tag{A-1}$$

$$\tilde{y}_{lp_i}(t) = \left[\sqrt{P_{C_i}} + j\sqrt{P_{D_i}}d(t)\left(\frac{4}{\pi}\right)\sum_{\substack{k=1\\ k\ odd}}^{M}\frac{\sin k\omega_{sc}t}{k}\right]e^{(j\omega t+\theta_i)} + \tilde{n}_{lp_i}(t) \tag{A-2}$$

where the subcarrier is expressed in terms of its sinusoidal components that are passed by the lowpass filter. The two signals passed through the bandpass filter of bandpass B_{bp} Hz contain only noise and are given by

$$\tilde{y}_{bp_i}(t) = \tilde{n}_{bp_1}(t) \tag{A-3}$$

$$\tilde{y}_{bp_i}(t) = \tilde{n}_{bp_i}(t) \tag{A-4}$$

The complex quantity used to estimate the relative signal phase $\phi_{1i} = \theta_1 - \theta_i$ is given by

$$\begin{aligned} Z &= I + jQ \\ &= \frac{1}{T_{corr}} \int \tilde{y}_{lp_1} \tilde{y}^*_{lp_i}\, dt - \frac{B_{lp}}{B_{bp}} \frac{1}{T_{corr}} \int \tilde{y}_{bp_1} \tilde{y}^*_{bp_i}\, dt \\ &= \left(\sqrt{P_{C_1} P_{C_i}} + \sqrt{P_{D_1} P_{D_i}} H\right) e^{j\phi_{1i}} + \frac{1}{T_{corr}} \int (\tilde{n}_{s,n} + \tilde{n}_{lp_1} \tilde{n}^*_{lp_i})\, dt - \frac{B_{lp}}{B_{bp}} \frac{1}{T_{corr}} \int \tilde{n}_{bp_1} \tilde{n}^*_{bp_i}\, dt \\ &= \left(\sqrt{P_{C_1} P_{C_i}} + \sqrt{P_{D_1} P_{D_i}} H\right) e^{j\phi_{1i}} + \tilde{N} \end{aligned} \tag{A-5}$$

In most cases, the contribution of the signal–noise term $\tilde{n}_{s,n}(t)$ to the total noise power is much smaller than that of the noise–noise terms, and can be ignored. This is especially true if the P_T/N_o levels of the two signals are very low, or if large correlation bandwidths are used. By the Central Limit Theorem, the complex noise $\tilde{N}$ can be approximated as Gaussian if the correlation extends over many independent samples (i.e., if T_{corr} is much greater than the inverse correlation bandwidths). After averaging, the variance of the real and imaginary parts of $\tilde{N}$ can be shown to be equal to

$$\lambda_I = Var(N_I) = \frac{1}{T_{corr}} \left(B_{lp} + \frac{B^2_{lp}}{B_{bp}}\right) (N_{o_1} N_{o_i} + \alpha^2_{1i} \cos 2\phi^n_{1i}) \tag{A-6}$$

$$\lambda_Q = Var(N_Q) = \frac{1}{T_{corr}} \left(B_{lp} + \frac{B^2_{lp}}{B_{bp}}\right) (N_{o_1} N_{o_i} - \alpha^2_{1i} \cos 2\phi^n_{1i}) \tag{A-7}$$

where N_I and N_Q are the real and imaginary parts of $\tilde{N}$, respectively. The covariance of N_I and N_Q can be shown to be equal to

$$\lambda_{IQ} = Cov(N_I,\ N_Q) = \frac{1}{T_{corr}} \left(B_{lp} + \frac{B^2_{lp}}{B_{bp}}\right) \alpha^2_{1i} \sin 2\phi^n_{1i} \tag{A-8}$$

Furthermore, it is clear from Eq. (A-5) that the means of the real and imaginary parts of Z are given by

$$m_I = \left(\sqrt{P_{C_1} P_{C_i}} + \sqrt{P_{D_1} P_{D_i}} H\right) \cos \phi_{1i} \tag{A-9}$$

$$m_Q = \left(\sqrt{P_{C_1} P_{C_i}} + \sqrt{P_{D_1} P_{D_i}} H\right) \sin \phi_{1i} \tag{A-10}$$

Equations (A-6), (A-7), (A-9), and (A-10) can be combined to compute the correlator SNR as defined in [1], i.e.,

$$SNR_{corr,fsc} = \frac{E[Z]E^*[Z]}{E[ZZ^*] - E[Z]E^*[Z]}$$

$$= \frac{m_I^2 + m_Q^2}{\lambda_I + \lambda_Q}$$

$$= \frac{T_{corr}}{2(B_{lp} + (B_{lp}^2/B_{bp}))} \left(\sqrt{\frac{P_{C_1}}{N_{o_1}} \frac{P_{C_i}}{N_{o_i}}} + \sqrt{\frac{P_{D_1}}{N_{o_1}} \frac{P_{D_i}}{N_{o_i}}} H \right)^2 \quad \text{(A-11)}$$

Equations (A-9), (A-10), and (A-6) through (A-8) can be used to determine the joint density function $p_{I,Q}(I,Q)$. Since the density of $\hat{\phi}_{1i} = \tan^{-1}(Q/I)$ is the desired quantity, we express the joint density function in terms of polar coordinates, using the variable definitions

$$r \triangleq \sqrt{I^2 + Q^2} \quad \text{(A-12)}$$

$$\phi \triangleq \tan^{-1}\left(\frac{Q}{I}\right) \quad \text{(A-13)}$$

The density function for jointly Gaussian random variables is given in polar form by

$$f_{r,\phi}(r,\phi) = \frac{r}{2\pi(\lambda_I\lambda_Q - \lambda_{IQ})} \times \exp\left(-\frac{\lambda_I(r\cos\phi - m_I)^2 - 2\lambda_{IQ}(r\cos\phi - m_I)(r\sin\phi - m_Q) + \lambda_Q(r\sin\phi - m_Q)^2}{2(\lambda_I\lambda_Q - \lambda_{IQ})} \right) \quad \text{(A-14)}$$

Integrating Eq. (A-14) with respect to r yields the marginal density of ϕ alone. Expressing the phase estimate density in terms of the estimation error $\Delta\phi = \hat{\phi}_{1i} - \phi_{1i}$ yields

$$f_\phi(\Delta\phi) = G_1 \exp\left(-SNR_{corr,fsc} \frac{1 - \rho^2\cos 2\psi}{1 - \rho^4} \right) \left[1 + \sqrt{\pi}\, G_2\, e^{G_2^2}\, \text{erf}\ G_2 + 1) \right] \quad \text{(A-15)}$$

where

$$G_1 = \frac{1 - \rho^4}{2\pi\,(1 - \rho^2\cos(2\psi - \Delta\phi))} \quad \text{(A-16)}$$

$$G_2 = \sqrt{SNR_{corr,fsc}} \frac{\cos\Delta\phi - \rho^2\cos(2\psi - \Delta\phi)}{(1 - \rho^4)(1 - \rho^2\cos(2\psi - \Delta\phi))} \quad \text{(A-17)}$$

Appendix B

Performance of the CSC Correlator

The method of estimating the relative signal phases for complex-symbol combining is analogous to the full-spectrum combining algorithm; using the extra correlation to compensate for the noise bias, the complex correlation can be expressed as

$$
\begin{aligned}
Z &= \frac{1}{N}\sum_{k=1}^{N}\tilde{Y}_1(k)\tilde{Y}_i^*(k) - \frac{1}{N}\sum_{k=1}^{N}\tilde{N}_1(k)\tilde{N}_i^*(k) \\
&= \sqrt{P_{D_1}P_{D_i}}\,\overline{C_{sc_1}}\,\overline{C_{sy_1}}\,\overline{C_{sc_i}}\,\overline{C_{sy_i}}e^{j\phi_{1i}} + \frac{1}{N}\sum_{k=1}^{N}\sqrt{P_{D_1}}C_{sc_1}C_{sy_1}e^{j\theta_1}\tilde{N}_i^*(k) \\
&\quad + \frac{1}{N}\sum_{k=1}^{N}\sqrt{P_{D_i}}C_{sc_i}C_{sy_i}e^{-j\theta_i}\tilde{N}_1^*(k) + \frac{1}{N}\sum_{k=1}^{N}\tilde{N}_1(k)\tilde{N}_i^*(k) - \frac{1}{N}\sum_{k=1}^{N}\tilde{N}_1'(k)\tilde{N}_i'^*(k) \\
&= \sqrt{P_{D_1}P_{D_i}}\,\overline{C_{sc_1}}\,\overline{C_{sy_1}}\,\overline{C_{sc_i}}\,\overline{C_{sy_i}}e^{j\phi_{1i}} + \tilde{N}
\end{aligned}
\tag{B-1}
$$

where N is the number of symbols averaged over, given by $N = T_{corr}/T_{sym}$, and the noise term $\tilde{N}$ has zero mean. The statistics of this noise can be analyzed in the same manner as before; here, the effective correlation bandwidth for both the lowpass and the bandpass correlation is $R_{sym}/2$. Using the definition given by Eq. (32), the correlator SNR can be shown to be equal to

$$
SNR_{corr,csc} = \frac{P_{D_1}}{N_{o_1}}\frac{T_{corr}\overline{C_{sc_1}}^2\,\overline{C_{sy_1}}^2\,\overline{C_{sc_i}}^2\,\overline{C_{sy_i}}^2}{\overline{C_{sc_i}^2}\,\overline{C_{sy_i}^2} + \overline{C_{sc_1}^2}\,\overline{C_{sy_1}^2}(1/\gamma_i) + (N_{o_i}/P_{D_i})2R_{sym}}
\tag{B-2}
$$

The density function for the phase estimation error can be found in a manner analogous to that applied in Appendix A. The only difference is in the expression for the correlator SNR; otherwise, both problems are inherently governed by the same mathematics. The density function for the phase estimation error $\Delta\phi_{1i}$ is thus given by Eq. (A-15), with $SNR_{corr,fsc}$ replaced by $SNR_{corr,csc}$.

A Seismic Data Compression System Using Subband Coding

A. B. Kiely and F. Pollara
Communications Systems Research Section

This article presents a study of seismic data compression techniques and a compression algorithm based on subband coding. The algorithm includes three stages: a decorrelation stage, a quantization stage that introduces a controlled amount of distortion to allow for high compression ratios, and a lossless entropy coding stage based on a simple but efficient arithmetic coding method. Subband coding methods are particularly suited to the decorrelation of nonstationary processes such as seismic events. Adaptivity to the nonstationary behavior of the waveform is achieved by dividing the data into separate blocks that are encoded separately with an adaptive arithmetic encoder. This is done with high efficiency due to the low overhead introduced by the arithmetic encoder in specifying its parameters. The technique could be used as a progressive transmission system, where successive refinements of the data can be requested by the user. This allows seismologists to first examine a coarse version of waveforms with minimal usage of the channel and then decide where refinements are required. Rate-distortion performance results are presented and comparisons are made with two block transform methods.

I. Introduction

A typical seismic analysis scenario involves collection of data by an array of seismometers, transmission over a channel offering limited data rate, and storage of data for analysis. Seismic data analysis is performed for monitoring earthquakes and for planetary exploration, as in the planned study of seismic events on Mars. Seismic data compression systems are required to cope with the transmission of vast amounts of data over constrained channels and must be able to accurately reproduce both low-energy seismic signals and occasional high-energy seismic events.

We describe a compression algorithm that includes three stages: a decorrelation stage based on subband coding, a uniform quantization stage, and a lossless entropy coding stage based on arithmetic coding. Rate-distortion performance results are presented and comparisons are made with two block transform methods: the discrete cosine transform (DCT) and the Walsh–Hadamard transform (WHT).

Subband coding methods are particularly suited to the decorrelation of nonstationary processes such as seismic events. For most seismic data, signal energy is more concentrated in the low-frequency subbands, which suggests the use of nonuniform subband decomposition. The decorrelation stage is implemented by quadrature mirror filters using a lattice structure. Adaptivity to the nonstationary behavior of the waveform is achieved by dividing the data into blocks that are separately encoded.